Wnt signaling dosage controlled by a *Ctnnb1* enhancer balances homeostasis and tumorigenesis of intestinal epithelia

Xiaojiao Hua[1,2], Chen Zhao[1,2], Jianbo Tian[4,5], Junbao Wang[1,2], Xiaoping Miao[4,5], Gen Zheng[6], Min Wu[2,3,5], Mei Ye[7], Ying Liu[1,2,*], Yan Zhou[1,2,*]

[1]Department of Neurosurgery, Medical Research Institute, Zhongnan Hospital of Wuhan University, Wuhan University, Wuhan, China

[2]Frontier Science Center of Immunology and Metabolism, Wuhan University, Wuhan, China

[3]College of Life Sciences, Wuhan University, Wuhan, China

[4]Department of Epidemiology and Biostatistics, School of Public Health, Wuhan University, Wuhan, China.

[5]TaiKang Center for Life and Medical Sciences, Wuhan University, Wuhan, China

[6]Department of Gastroenterology, Union Hospital, Tongji Medical College, Huazhong University of Science and Technology, Wuhan, China

[7]Department of Gastroenterology, Zhongnan Hospital of Wuhan University, Wuhan, China

*Correspondence to Dr. Ying Liu, y.liu@whu.edu.cn; Dr. Yan Zhou, yan.zhou@whu.edu.cn

Abstract

The β-catenin-dependent canonical Wnt signaling is pivotal in organ development, tissue homeostasis, and cancer. Here we identified an upstream enhancer of *Ctnnb1*, named ieCtnnb1, that is crucial for intestinal homeostasis. ieCtnnb1 is predominantly active in the base of small intestinal crypts and throughout the epithelia of large intestine. Knockout of ieCtnnb1 led to a reduction in *Ctnnb1* transcription, compromising the canonical Wnt signaling in

intestinal crypts. Single-cell sequencing revealed that ieCtnnb1 knockout altered epithelial compositions and potentially compromised functions of small intestinal crypts. While deletion of ieCtnnb1 hampered epithelial turnovers in physiologic conditions, it prevented occurrence and progression of Wnt/β-catenin-driven colorectal cancers. Human ieCTNNB1 drove reporter gene expression in a pattern highly similar to mouse ieCtnnb1. ieCTNNB1 contains a single-nucleotide polymorphism associated with *CTNNB1* expression levels in human gastrointestinal epithelia. The enhancer activity of ieCTNNB1 in colorectal cancer tissues was stronger than that in adjacent normal tissues. HNF4α and phosphorylated CREB1 were identified as key trans-factors binding to ieCTNNB1 and regulating *CTNNB1* transcription. Together, these findings unveil an enhancer-dependent mechanism controlling the dosage of Wnt signaling and homeostasis in intestinal epithelia.

Introduction

The gastrointestinal (GI) epithelium, a high turnover organ, contains multiple cell types to fulfill complex functions including food digestion, nutrient absorption, pathogen insulation and clearance, as well as endocrine roles (**Chin et al., 2017; Kurokawa et al., 2020; Noah et al., 2011**). Enterocytes (ECs) constitute ~90% of all differentiated cells and function as highly efficient cells for absorbing nutrients and water (**Snoeck et al., 2005**). Goblet cells (GCs) produce mucus to lubricate the mucosal surface **(Gustafsson & Johansson, 2022**). Enteroendocrine cells (EECs) sense luminal nutrients and secrete peptide hormones to regulate appetite, intestinal motility, and insulin release (**Gribble & Reimann, 2019**). Tuft cells (TCs) are chemosensory cells that respond to various stimuli including infections and hypoxia (**Schneider et al., 2019**). The crypts of GI epithelium harbor various types of stem cells that continually replenish lost epithelial cells (**Ramadan et al., 2022; van der Flier & Clevers, 2009**). While the prevailing belief is that *Lgr5*-expressing crypt base

columnar (CBC) cells are actively dividing stem cells and *Bmi*-expressing "+4" cells (positioned four cells above the base of the crypt) are slowly cycling stem cells, it's important to note that crypt cells have the capacity for fate reprogramming and de-differentiation to sustain regenerative capability (**Barker et al., 2007; Beumer & Clevers, 2016; Metcalfe et al., 2014; Tian et al., 2011; Yan et al., 2012**). Intestinal stem cells generate transit-amplifying cells (TACs), which undergo multiple cell divisions and differentiate into all intestinal lineages while migrating towards the crypt orifice (**Krausova & Korinek, 2014**). In addition to stem and progenitor cells, the base of small intestinal crypts contains Paneth cells (PCs) that secret antimicrobial peptides, called defensins, thereby contributing to host defense against microbes (**Barreto et al., 2022; Lueschow & McElroy, 2020**). PCs also contribute to the stem cell niche function, *e.g.* secreting Wnt ligands, to maintain epithelial homeostasis of the small intestine (**Sato et al., 2011**).

The behavior of crypt cells is precisely regulated by multiple signals, which can act sequentially, additively, synergistically, or antagonistically (**Nakamura et al., 2007)**. Among them, the Wnt/β-catenin signal pathway represents the principal force governing intestinal epithelium homeostasis, particularly in the preservation of stem cell proliferation and multipotency (**Clevers et al., 2014; Mah et al., 2016; Pinto et al., 2003**). Upon Wnt ligand binding, the β-catenin degradation complex is inactivated, leading to accumulation of β-catenin and its translocation into the nucleus, where it works with the co-activator TCF-4 to turn on the transcription of a plethora of target genes, including *c-Myc*, *CCND1*, *AXIN2*, and *CD44* (**Clevers, 2006; Clevers & Nusse, 2012; Nusse & Clevers, 2017**). Inhibition of Wnt ligand secretion reduced number of functional stem cells and led to a faster crypt fixation rate (**Huels et al., 2018**). In the process of aging, reduced Wnt signaling in stem cells and the niche of intestinal crypts causes inhibition of proliferation and reduced numbers of intestinal stem cells (**Nalapareddy et al., 2017; Pentinmikko et al., 2019**). The Wnt signal is also

essential for commitment, maturation, and location of PCs and other secretory cells (**Andreu et al., 2008; van Es et al., 2005**). On the other hand, Wnt, EGF and Delta-like 1/4 ligands presented by PCs sustained CBCs' proliferative states and the production (**Sato et al., 2011**). Although the Wnt signal dosage, largely *via* post-translational regulations, controls early lineage specification, hematopoiesis, and tumorigenesis (**Bakker et al., 2013; Luis et al., 2011**), it remains elusive how Wnt signaling dosage, particularly through the transcriptional control of *Ctnnb1*, regulates composition and function of intestinal epithelia.

Aberrant activation of canonical Wnt signaling is associated with GI cancers, most notably colorectal cancer (CRC) (**Zhao et al., 2022; Zhu & Li, 2023**). Germinal mutations of the *APC* gene, which encodes the negative regulator of β-catenin, underlie the Familial Adenomatous Polyposis (FAP), a hereditary neoplastic syndrome and the pre-cancerous condition for CRC (**Cheng et al., 2019; J. Li et al., 2021**). Moreover, *APC* is mutated in up to 80% of human sporadic CRCs (**J. Li et al., 2021**). Inactivation of APC causes enhanced accumulation of β-catenin in nuclei and subsequent activation of proliferative and pro-survival signals in CRC cells (**Cheng et al., 2019**). However, largely due to lack of specificity, no molecular therapeutic strategy targeting the pathway has been incorporated into CRC treatment. Interestingly, the transcriptional activity of *CTNNB1*, the coding gene for β-catenin, is also enhanced in CRCs (**Terrin et al., 2017**); however, the underlying mechanism is largely unknown. Dissecting it would facilitate the development of new Wnt/β-catenin targeting means to treat CRC.

Enhancers are essential *cis*-regulatory DNA elements that control spatiotemporal gene expressions during cell fate specification and maintenance (**Pachano et al., 2022**). Active enhancers are often associated with cell fate specifiers, mostly transcription factors (TFs), and are enriched with specific histone modification such as H3K27ac (acetylated lysine 27 of histone

H3) and H3K4me1 (mono-methylated lysine 4) of histone H3 (**Jindal & Farley, 2021**). Importantly, variations of enhancer sequences often lead to aberrant gene silence and activation, thereby causing developmental anomalies and cancers (**Kvon et al., 2021; Sengupta & George, 2017; Zabidi & Stark, 2016**). Although numerous putative enhancers have been identified by high-throughput studies, only a fraction of them were functionally annotated.

The proper expression of essential fate genes in different cell types is often controlled by specific enhancers(**Kvon et al., 2021; Pachano et al., 2022**). We previously identified a neocortical enhancer of *Ctnnb1*, the coding gene of β-catenin. The enhancer – neCtnnb1, is specifically active in the subventricular zone of developing neocortex and regulates the abundance of intermediate progenitors and production of superficial-layer pyramidal neurons (**Wang et al., 2022**). Here we have identified an intestinal enhancer for *Ctnnb1* and name it as ieCtnnb1. Reporter mice showed that ieCtnnb1 is predominantly active in the base of small intestinal crypts and across the epithelium of large intestine. Knockout of ieCtnnb1 slows down turnovers of intestinal epithelia at physiology and cancer conditions in a Wnt/β-catenin dependent manner. The human ieCTNNB1 contains a SNP that is associated with *CTNNB1* expression levels in human gastrointestinal epithelia. The enhancer activity of ieCTNNB1 in CRC tissues is higher than that in adjacent normal tissues and positively correlates with *CTNNB1* expression levels. HNF4α and phosphorylated CREB1 at serine 133 (p-S133-CREB1) were found to associate with ieCtnnb1 and regulate *Ctnnb1* transcription.

Results

ieCtnnb1 is a gastrointestinal enhancer of *Ctnnb1*

We previously identified an evolutionarily conserved upstream enhancer for *Ctnnb1* – neCtnnb1, which regulates neocortical neurogenesis (**Figure 1 - figure supplement 1A**). We reasoned that there might be other potential

146 enhancer regions that control *Ctnnb1* expression in a cell-specific manner.
147 Therefore, we scanned upstream regions of *Ctnnb1* for active enhancer
148 properties – open chromatin with enriched H3K27ac and H3K4me1 – in
149 different tissues using data retrieved from the ENCODE database. Interestingly,
150 we noticed that a region that is 29,068 base pair (bp) upstream of the
151 transcription starting site (TSS) for *Ctnnb1* displayed typical enhancer feature
152 in intestinal tissues and resides in the same topologically associating domain
153 (TAD) with *Ctnnb1* (**Figure 1A, Figure 1 - figure supplement 2A**). The region,
154 named as ieCtnnb1 (intestinal enhancer of *Ctnnb1*), is at open chromatin status
155 (DNase I hypersensitive site) and enriched with H3K27ac and H3K4me1, two
156 histone marks for active enhancers, in 8-week-old mouse small intestine tissue
157 (**Figure 1A**). Importantly, the enrichment of H3K27ac at ieCtnnb1 is also
158 prominent in embryonic intestine and stomach tissue, as well as in adult kidney
159 and liver (**Figure 1 - figure supplement 1B and D**). In contrast, the enrichment
160 was not detected in non-gastrointestinal tissues such as embryonic and adult
161 brain (**Figure 1 - figure supplement 1D**). In line with signatures of active
162 enhancers, the enrichment of H3K4me3 and H3K36me3 at ieCtnnb1 is
163 negligible in all examined tissues (**Figure 1A, Figure 1 - figure supplement**
164 **1B and C**).

165 We next performed *in vitro* and *in vivo* analyses to validate ieCtnnb1's
166 enhancer activity. First, the 2,153 bp core region (CR), representing the
167 H3K27ac peak region of ieCtnnb1, could drive the expression of luciferase
168 reporter in multiple cell types (**Figure 1 - figure supplement 2B**). Second, the
169 ieCtnnb1 reporter mice (*H11*$^{i.enh}$) were constructed by inserting the reporter
170 cassette – 5'-*Shh*'s promoter-ieCtnnb1-CR-*LacZ*-*iCre*-3' – into the *H11* locus
171 (**Figure. 1B**). Of note, the *Shh* promoter alone at the *H11* locus did not drive
172 the expression of reporter gene in all examined tissue (**Kvon et al., 2020**).
173 Wholemount β-galactosidase (β-gal) staining of 8-week-old tissues revealed
174 prominent ieCtnnb1-*LacZ* signals along the gastrointestinal (GI) tract. The

175 signal exhibited a proximal-low to distal-high gradient, with the ileum, cecum,
176 and colon showing the strongest signals (**Figure. 1B, Figure 1 - figure**
177 **supplement 2C**). The stomach and proximal duodenum also displayed
178 reporter activity driven by ieCtnnb1 (**Figure. 1B, Figure 1 - figure supplement**
179 **2C**). β-gal staining of intestinal sections revealed that the ieCtnnb1-*LacZ* signal
180 could be visualized at the bottom of small intestinal crypts and in the entire large
181 intestinal epithelia, but is absent in sections of liver, kidney, and spleen (**Figure**
182 **1 - figure supplement 2D and data not shown**). Interestingly, the proximal-
183 low to distal-high gradient of ieCtnnb1-*LacZ* signal along the small intestine
184 corresponds to the expression pattern of β-catenin (**Figure 1 - figure**
185 **supplement 2E**).

186 The transcription activity of ieCtnnb1 is strongest at the bottom of crypts,
187 where *Lgr5*-expressing CBC cells and Paneth cells (PCs) reside. To more
188 precisely elucidate cell types in which ieCtnnb1 is active, we crossed $H11^{i.enh}$
189 mice with *Lgr5*-EGFP-IRES-CreERT2 (*Lgr5*-EGFP) mice to obtain 8-week-old
190 $H11^{i.enh}$;*Lgr5-EGFP* mice. Small intestinal crypts were respectively harvested
191 from *Lgr5-EGFP* and $H11^{i.enh}$;*Lgr5-EGFP* mice followed by enrichment of both
192 eGFP+ and eGFP- cells (**Figure 1 - figure supplement 2F**). Quantitative RT-
193 PCR (RT-qPCR) analyses indicated that *LacZ* transcripts could be detected in
194 both eGFP+ and eGFP- crypt cells in $H11^{i.enh}$;*Lgr5-EGFP* mice (**Figure 1 -**
195 **figure supplement 2F**). Next, sections of $H11^{i.enh}$ crypts were subjected with
196 β-gal staining followed by immunohistochemistry of OLFM4 (a CBC marker) or
197 lysozyme (a PC marker). Data showed X-gal signals are in close proximity with
198 both OLFM4 and lysozyme (**Figure. 1C**), suggesting that the activity of
199 ieCtnnb1 is present in both CBCs and PCs.

200 We further examined the ieCtnnb1 activity in GI tracts of postnatal day 7
201 (P7) pups, when GI epithelia are rapidly expanding. The ieCtnnb1-*LacZ* signals
202 could be visualized in epithelia of P7 small and large intestines, aligning well
203 with the distribution of canonical Wnt signaling illustrated by the BAT-Gal mice

204 (**Figure 1 - figure supplement 2G and H**). Together, ieCtnnb1 drives
205 transcription in embryonic intestinal epithelia, the base of small intestinal crypts
206 and large intestinal epithelia of adult mice.
207

208 **ieCtnnb1 maintains the expression of *Ctnnb1* in intestinal epithelia**

209 We next examined whether ieCtnnb1 controls the transcription of *Ctnnb1*
210 in intestinal epithelia. For this purpose, we employed CRISPR/Cas9-mediated
211 gene editing to delete the genomic region containing ieCtnnb1 (**Figure 1 -**
212 **figure supplement 2I**). Homozygous ieCtnnb1 knockout (*Ctnnb1*$^{\Delta i.enh}$) mice
213 were born in Mendelian ratios and thrived through adulthood. Interestingly, the
214 body weight of 8-week-old male *Ctnnb1*$^{\Delta i.enh}$ mice was slightly but significantly
215 lighter than that of wildtype controls (**Figure. 1D and F**), but the length of small
216 and large intestines of *Ctnnb1*$^{\Delta i.enh}$ mice was comparable to that of control mice
217 (**Figure. 1E, G and H**). We then collected crypts from small and large intestine,
218 finding that the expression levels of *Ctnnb1* were decreased by 26.5% and 22.3%
219 respectively in *Ctnnb1*$^{\Delta i.enh}$ crypts (**Figure. 1I and J**). In contrast, the expression
220 level of *Ctnnb1* in the *Ctnnb1*$^{\Delta i.enh}$ liver remained unaltered (**Figure 1 - figure**
221 **supplement 2J**). In addition, the expression of genes located in the same TAD
222 as *Ctnnb1* and ieCtnnb1, including *Ulk4*, *Rpl14* and *Entpd3*, was not changed
223 in *Ctnnb1*$^{\Delta i.enh}$ small intestinal crypts (**Figure 1 - figure supplement 2K**). These
224 data suggest that ieCtnnb1 specifically maintains *Ctnnb1*'s transcription in
225 intestinal epithelia.

226 In epithelial tissues, most β-Catenin is localized at cell adhesion sites to
227 maintain barrier integrity, while a smaller fraction translocates into the nucleus
228 to active transcription upon Wnt ligand binding. We therefore carried out
229 nuclear/cytosol fractionation assays, which revealed a more substantial
230 decrease in the level of nuclear β-Catenin compared to cytosolic β-Catenin
231 (49.5% versus 29.8%) in small intestinal crypts of *Ctnnb1*$^{\Delta i.enh}$ mice (**Figure. 1K**
232 **and L**). RNA-seq transcriptome and RT-qPCR analyses revealed a significant

233 reduction in the expression levels of components in the Wnt signaling pathway,
234 as well as Wnt target genes, in *Ctnnb1*$^{\Delta i.enh}$ crypts (**Figure. 1M and N**).
235 Together, the loss of ieCtnnb1 undermined the Wnt signaling in intestinal
236 epithelia by reducing *Ctnnb1* transcription.
237
238 **Loss of ieCtnnb1 altered cellular composition and expression profiles of**
239 **small intestinal crypts**
240 The canonical Wnt/β-catenin signaling is essential for the construction and
241 homeostasis of intestinal epithelia (**Mah et al., 2016**). Because ieCtnnb1
242 maintains the expression level of *Ctnnb1* of intestinal crypts, we investigated
243 how the deletion of ieCtnnb1 affects cellular components and functions of
244 intestinal crypts. We performed single-cell sequencing on EpCAM+ epithelial
245 cells from small intestinal crypts of 10-week-old *Ctnnb1*$^{\Delta i.enh}$ and control
246 (*H11*$^{i.enh}$) mice (n = 2 female mice for each genotype) (**Figure. 2A, Figure 2 -**
247 **figure supplement 1A**) (**Ayyaz et al., 2019**). Uniform Manifold Approximation
248 and Projection (UMAP) was employed for dimensionality reduction to cluster
249 cells, then well-established marker genes were mapped onto the UMAP
250 representation to designate cell types (**Haber et al., 2017**) (**Figure. 2B, Figure**
251 **2 - figure supplement 1B-D**). A small population of crypt cells could not be
252 clearly defined probably due to certain technical issues during crypt extraction,
253 antibody staining, or cell sorting (**Figure 2 - figure supplement 1D**). First, in
254 accordance with bulk RNA-seq and RT-qPCR results, the expression levels of
255 *Ctnnb1* were downregulated in almost all *Ctnnb1*$^{\Delta i.enh}$ crypt cells, and the
256 expression of *Axin2* was decreased in CBCs and TACs (**Figure. 2C and D**).
257 Second, the proportion of PCs was decreased by 49.2% in *Ctnnb1*$^{\Delta i.enh}$ crypts,
258 which was confirmed by the immunohistochemical (IHC) staining of *Defensin*
259 *5α*, a PC marker (**Figure. 2E and F**). The ieCtnnb1-driving *LacZ* could be
260 detected in the PC cluster (n = 4 10-week-old mice) (**Figure 2 - figure**
261 **supplement 1E**). Accordingly, the expression levels of examined PC markers

262 – *Lyz1*, *Pla2g2a*, *Wnt3* and *Math1* - were all significantly compromised in
263 *Ctnnb1*$^{\Delta i.enh}$ crypts (**Figure. 2G**). The number of goblet cells (GCs) was slightly
264 (not statistically significant) reduced upon loss of ieCtnnb1 (**Figure 2 - figure**
265 **supplement 1F**). Third, the proliferative capability of CSCs and TACs were
266 compromised in *Ctnnb1*$^{\Delta i.enh}$ crypts, as the proportion of G2/M cells and the
267 expression of *Mki67* were decreased in the two cell types (**Figure. 2H-J**).
268 Consistently, the numbers of Ki67-positive cells and EdU-labeled cells (4 hours
269 pulse) were decreased by 16.1% and 21.9%, respectively, in *Ctnnb1*$^{\Delta i.enh}$ small
270 intestinal epithelia (**Figure. 2K and L**). Fourth, in secretory cells (PCs GCs and
271 EECs), as well as enterocytes/absorptive cells (mature enterocytes (mECs)
272 and immature enterocytes (imECs)), and stem cells of *Ctnnb1*$^{\Delta i.enh}$ crypts, the
273 expression of genes related to secretory functions including *Lyz1*, *Ang4*, *Muc2*,
274 and *Mmp7* was decreased. In contrast, the expression of markers for absorptive
275 cells such as *Fabp6*, *Apoa1*, *Fabp2*, and *Reg3b* was elevated (**Figure. 2M and**
276 **N, Figure 2 - figure supplement 1G**). Accordingly, gene ontology (GO)
277 analyses showed in stem cells and secretory cells of *Ctnnb1*$^{\Delta i.enh}$ crypts,
278 upregulated genes were enriched with terms associated with absorptive
279 functions including ribosome biogenesis and oxidative phosphorylation;
280 whereas downregulated genes in stem cells and secretory cells were
281 respectively enriched with terms related to cell division and secretory functions
282 (**Figure 2 - figure supplement 1H and I**). In contrast, in mECs, downregulated
283 genes were enriched with terms associated with absorptive functions (**Figure 2**
284 **- figure supplement 1J**).
285 In summary, the loss of ieCtnnb1 results in a reduction in the number of
286 PCs, compromises stem cell proliferation, and disrupts the expression of genes
287 related to secretory and absorptive functions. These effects could be attributed
288 to a combination of reduced Wnt/β-catenin signaling and dysregulated
289 crosstalk among crypt cells.
290

291 **ieCtnnb1 deletion inhibits tumorigenesis of intestinal cancers by**
292 **suppressing Wnt/β-catenin signaling**

293 Tumorigenesis of most colorectal cancer (CRC) is associated with aberrant
294 activation of the Wnt/β-catenin signaling (**Zhu & Li, 2023**). To investigate
295 whether knockout of ieCtnnb1 could suppress the carcinogenesis of Wnt-driven
296 intestinal tumors, we crossbred *Ctnnb1*$^{\Delta i.enh}$ mice with *Apc*$^{Min/+}$ mice. In *Apc*$^{Min/+}$
297 mice, a nonsense mutation of the *Apc* gene results in the translation of
298 truncated and dysfunction APC protein, leading to failed degradation and
299 nuclear translocation of β-catenin. *Apc*$^{Min/+}$ mice spontaneously develop
300 intestinal tumors due to enhanced canonical Wnt/β-catenin signaling in the
301 intestinal epithelia, particularly in stem cells (Su et al., 1992). The survival
302 period of *Ctnnb1*$^{\Delta i.enh}$;*Apc*$^{Min/+}$ mice (median survival - 255 days) was
303 significantly longer than the *Apc*$^{Min/+}$ mice (median survival - 165 days), with the
304 former having a heavier body weight (**Figure. 3A and C**). Strikingly, the
305 *Ctnnb1*$^{\Delta i.enh}$;*Apc*$^{Min/+}$ mice barely grow colorectal cancers and have much fewer
306 intestinal tumors compared to *Apc*$^{Min/+}$ mice, with significantly smaller tumor
307 area (**Figure. 3B, D-F, Figure 3 - figure supplement 1A-C**). IHC analyses
308 showed that tumors in *Ctnnb1*$^{\Delta i.enh}$;*Apc*$^{Min/+}$ large and small intestines had much
309 fewer Ki67+ proliferating cells, expressed significant less β-catenin, but
310 contained more Muc2-expressing Goblet cells, suggesting *Ctnnb1*$^{\Delta i.enh}$;*Apc*$^{Min/+}$
311 tumors behave like normal epithelia (**Figure. 3G-L, Figure 3 - figure**
312 **supplement 1D-I**)**.** Consistently, RNA-seq transcriptome experiments showed
313 that *Ctnnb1*$^{\Delta i.enh}$;*Apc*$^{Min/+}$ colorectal cancers significantly downregulated genes
314 associated with the Wnt signaling pathway, pluripotency of stem cells, and
315 gastric cancer; whereas increased expression of genes related to normal
316 epithelial functions including oxidative phosphorylation, adhesion, protein
317 digestion and absorption, and Mucin biosynthesis (**Figure. 3M-O**). Thus,
318 ablation of ieCtnnb1 deters tumorigenesis of intestinal cancers by suppressing
319 the Wnt signaling.

320

321 **Human ieCTNNB1 drives the expression of reporter gene in the**
322 **gastrointestinal tract**

323 We next investigated whether the human genome also harbors an
324 intestinal enhancer for *CTNNB1*. A region with open chromatin (DNase I
325 hypersensitivity) and enrichment of H3K27ac/H3K4me1 was identified at
326 38,489 bp upstream of human *CTNNB1* in adult small intestine and colon
327 tissues (**Figure. 4A**). Moreover, the H3K27ac enrichment is also present in
328 esophagus but not in non-GI tissues (**Figure 4 - figure supplement 1A**).
329 Similar to ieCtnnb1, the 3 kb-long human genomic region, named as ieCTNNB1,
330 resides in the same TAD as the promoter of *CTNNB1* (**Figure 4 - figure**
331 **supplement 1B**). We generated ieCTNNB1 reporter mice (*H11*$^{hi.enh}$) and
332 observed that ieCTNNB1 could drive *LacZ* expression in the bottom of small
333 intestinal crypts and the entire epithelia of large intestine, also exhibiting a
334 proximal-low to distal-high pattern (**Figure. 4B**). Notably, the LacZ signal driven
335 by human ieCTNNB1 was less intense than that driven by mouse ieCtnnb1,
336 potentially attributed to species-specific TF-enhancer interactions.

337 The H3K27ac-enriched region of ieCTNNB1 was divided into five equal
338 parts for the luciferase reporter assay. Experiments demonstrated that each of
339 the five ieCTNNB1 subregions individually increased luciferase activity in both
340 HCT116 and HeLa cells (**Figure. 4C, Figure 4 - figure supplement 1C**)**.** We
341 then conducted CRISPR mediated activation and interference in HCT-15
342 colorectal cancer cells using three guide RNAs (gRNAs) targeting ieCTNNB1,
343 which respectively enhanced and inhibited transcription of *CTNNB1* (**Figure.**
344 **4D**). Together, ieCTNNB1 is the intestinal enhancer of *CTNNB1* for human GI
345 epithelia.

346

347 **ieCTNNB1 is activated in colorectal cancer and its activity positively**
348 **correlates with the expression of *CTNNB1***

CRC, one of the most prevalent cancers in human, is often associated with aberrant activation of the Wnt signaling (**J. Li et al., 2021**). We then studied whether the occurrence of CRC is associated with enhancer activation of ieCTNNB1. We performed paired analyses of chromatin immunoprecipitation sequencing (ChIP-seq) and RNA-seq data derived from 68 CRC samples and their neighboring normal (native) tissue (**Figure. 5A, Figure 5 - figure supplement 1A**). As anticipated, the expression levels of *CTNNB1* in CRC samples are significantly higher than those in neighboring native tissues (**Figure. 5B**). Essentially, the enrichment of H3K27ac at ieCTNNB1 in CRC tissues were significantly higher than that in native tissues (**Figure. 5C，Figure 5 - figure supplement 1A**). In contrast, the enrichment of H3K4me3 at *CTNNB1*'s promoter was comparable between cancer and native tissues (**Figure. 5C**). Moreover, the enrichment of H3K27ac at ieCTNNB1 positively correlated with the expression of *CTNNB1*; but the enrichment of H3K4me3 at *CTNNB1*'s promoter was not associated with *CTNNB1*'s expression (**Figure. 5D**). Therefore, it's the activity of enhancer but not the promoter that reflects the occurrence of CRC and expression levels of *CTNNB1*.

By examining Genotype Tissue Expression (GTEx) eQTL data browser, a single-nucleotide polymorphism (SNP) – rs15981379 (C>T) within ieCTNNB1 was discovered (**Figure. 5A**). Importantly, the C>T variation is inversely correlated with expression levels of *CTNNB1* in the esophagus and transverse colon (**Figure. 5E**). Luciferase reporter assays in HCT116 and HeLa cells revealed that the C>T variation indeed compromised luciferase activity driven by the ieCTNNB1-region 1 (**Figure. 5F**).

HNF4α and p-S133-CREB1 bind to ieCTNNB1 and maintains the expression of *CTNNB1*

Characterizing associated trans-factors of ieCtnnb1 and ieCTNNB1 is essential for revealing related transcriptional mechanisms and holds clinical

378 relevance. By examining Cistrome Data Browser for ChIP-seq data, eight trans-
379 factors were found to associate with ieCTNNB1 in human colorectal cancer
380 cells or ieCtnnb1 in mouse GI tissues (**Figure. 6A, Figure 6 - figure**
381 **supplement 1A**). Moreover, they are relatively highly expressed and/or have
382 positive correlation with *CTNNB1*'s expression in colon cancer samples. We
383 then transduced shRNAs-expressing plasmids into HCT-15 cells to individually
384 down-regulate their expressions, revealing that decreasing the expression of
385 *CREB1* (cAMP responsive element binding protein 1) or *HNF4A* (hepatocyte
386 nuclear factor 4 alpha) could compromise *CTNNB1*'s transcription (**Figure. 6B,**
387 **Figure 6 - figure supplement 1B**). Of note, HNF4α plays crucial roles in the
388 normal development of the colon and the maintenance of epithelial barrier
389 (**Cattin et al., 2009; Garrison et al., 2006**). The phosphorylation of CREB1 at
390 serine 133 (p-S133-CREB1) is essential for its role in activation of gene
391 transcription (**Carlezon et al., 2005**). ChIP-qPCR experiments showed that
392 enrichment of p-S133-CREB1 was more prominent than CREB1 at ieCtnnb1 in
393 small intestinal crypts and at ieCTNNB1 in HCT-15 cells (**data not shown**).
394 Notably, HNF4α and p-S133-CREB1 bind to multiple subregions of ieCTNNB1
395 and ieCtnnb1, as well as the promoters of *CTNNB1* and *Ctnnb1* (*pCTNNB1* and
396 *pCtnnb1*) in HCT-15 cells and small intestinal crypts (**Figure. 6C and D, Figure**
397 **6 - figure supplement 1C and D**). By analyzing the GEIPA-COAD (colon
398 adenocarcinoma) and READ (rectum adenocarcinoma) database, expression
399 levels of *CREB1* and *HNF4A* were found to be significantly higher in colon and
400 rectum cancer samples than those of normal tissues (**Figure. 6E**). Furthermore,
401 expression levels of *CREB1* and *HNF4A* positively correlated with that of
402 *CTNNB1* (**Figure. 6F**). HNF4α and p-S133-CREB1 were significantly enriched
403 at the promoter of *Ctnnb1* in *Apc* mutation induced colon cancer tissues (**Figure.**
404 **6G and H**). Intriguingly, knockout of ieCtnnb1 greatly diminished the
405 association of HNF4α and p-S133-CREB1 with *Ctnnb1*'s promoter (**Figure. 6G**
406 **and H**). In summary, HNF4α and p-S133-CREB1 were identified as essential

407 trans-factors that bind to ieCTNNB1 and maintain *CTNNB1*'s expression.

408

409 **Discussion**

410 The intestinal epithelia replenish themselves rapidly throughout lifetime,
411 which enables regeneration while predisposes to GI cancers (**Clevers, 2013**).
412 The optimal strength and dynamics of canonical Wnt/β-catenin signaling is
413 central to both homeostasis and tumorigenesis of GI tracts (**Beumer & Clevers,**
414 **2016; Pinto et al., 2003; Silvia Maretto, 2003**). While the stabilization and
415 nuclear translocation of β-catenin is the key step for Wnt signaling activation,
416 the transcriptional control of *Ctnnb1* could be another layer of regulation **(Rim**
417 **et al., 2022; Zhang & Wang, 2020**). Here we unveiled an enhancer-dependent
418 transcriptional machinery that tunes expressions of *Ctnnb1* in multiple cell types
419 of intestinal crypts, thereby balancing homeostasis and tumorigenesis of
420 intestinal epithelia (**Figure supplement 8**).

421 Our findings reinforce the notion that the canonical Wnt signaling is
422 required for the establishment of the secretory cell lineage (**Pinto & Clevers,**
423 **2005; Pinto et al., 2003; van Es et al., 2005**). Expression levels of markers for
424 secretory cells were greatly reduced whereas levels of markers for absorptive
425 cells were elevated in all small intestinal crypt cells of *Ctnnb1*$^{\Delta i.enh}$ mice. Fate
426 determinations of CBC daughter cells occur upon leaving the stem cell niche,
427 exposed to changing WNT, Notch and EGF levels. Progenitors losing contact
428 with PC Notch ligands upregulate DLL1 and DLL4, commit to the secretory
429 lineage, and induce Notch activity in neighboring cells, promoting enterocyte
430 differentiation (**Beumer & Clevers, 2020; van Es et al., 2012**).

431 WNT signaling not only directs PC-fated progenitors toward the crypt
432 bottom but also directly induces their differentiation (**Andreu et al., 2008;**
433 **Beumer & Clevers, 2020; van Es et al., 2005**). Single-cell sequencing and
434 reporter gene analyses indicated that the activity of ieCtnnb1 is present in PCs.
435 Knockout of ieCtnnb1 decreases number of PCs by almost 50% but the pool

436 size of CBCs was not significantly altered. A previous study showed that genetic
437 removal of PCs leads to the concomitant loss of Lgr5+ stem cells (**Sato et al.,**
438 **2011**), while other studies indicated that PCs are not mandatory niche cells for
439 the intestinal epithelia (**Durand et al., 2012; Garabedian et al., 1997; Kim et**
440 **al., 2012**). Although Wnt ligands provided by PCs may support Lgr5+ CBCs[32],
441 essential Wnt ligands are primarily supplied by subepithelial stromal
442 populations (**Degirmenci et al., 2018; Shoshkes-Carmel et al., 2018**). The
443 presence of redundancy at the stem cell niche enhances the accuracy in
444 maintaining intestinal homeostasis.

445 ieCtnnb1 knockout compromises Wnt signaling dosage, leading to PC loss,
446 dysregulation of genes controlling absorptive and secretory functions of
447 intestinal epithelia, and reduced proliferation of stem cells. These combined
448 effects could account for the lighter body weight observed in adult *Ctnnb1*$^{\Delta i.enh}$
449 mice.

450 On the other hand, colon and small intestinal tumors were rarely observed
451 in *Ctnnb1*$^{\Delta i.enh}$;*Apc*$^{Min/+}$ mice. Among the few *Ctnnb1*$^{\Delta i.enh}$ tumors analyzed, they
452 exhibited lower *Ctnnb1* expression, reduced proliferation, and behaved more
453 like normal intestinal epithelia. Different truncations or mutations of *APC* lead
454 to specific tumor types throughout the body in a Wnt/β-catenin dosage-
455 dependent manner. For example, although *Apc*^{1638N};*Ctnnb1*$^{+/-}$ mice were less
456 prone to GI cancers, *Apc*^{1638N};*Ctnnb1*$^{+/-}$ female animals tended to grow breast
457 cancers (**Bakker et al., 2013**). Therefore, the intestinal specificity of ieCtnnb1
458 makes it an ideal target to lower the strength of Wnt signaling in treating
459 colorectal cancer without affecting other tissues (**Hamdan & Johnsen, 2019;**
460 **Orouji, 2022**).

461 Both mouse ieCtnnb1 and human ieCTNNB1 were able to drive reporter
462 gene expression at the base of small intestinal crypts and throughout the
463 epithelium of the large intestine. Very intriguingly, unlike the highly conserved
464 neCtnnb1 sequence among amniotes, mouse ieCtnnb1 and human ieCTNNB1

465 do not share significant homology in primary sequence (**Wang et al., 2022**).
466 Nonetheless, both ieCtnnb1 and ieCTNNB1 localize at the intergenic region 30-
467 40 kb upstream of *Ctnnb1*'s promoter. Moreover, both ieCtnnb1 and ieCTNNB1
468 contain binding motifs for HNF4α and CREB1. HNF4α and p-S133-CREB1
469 were found to associate with ieCtnnb1 and *Ctnnb1*'s promoter to maintain
470 *Ctnnb1*'s expression. These findings support the notion that conserved TF
471 binding motifs stabilize and preserve enhancer functionality over evolution
472 **(Wong et al., 2020; Zabidi & Stark, 2016)**. Future studies could dissect how
473 sequence variations of ieCtnnb1 are adapted to intestinal homeostasis of
474 different species.
475

476 **Methods**

477 **Mice and genotyping**

478 All animal procedures were approved by the Animal Care and Ethical
479 Committee of Medical Research Institute at Wuhan University. C57BL/6 back-
480 ground mice were housed in a temperature- and humidity- controlled
481 environment with 12hr light/dark cycle and food/water ad libitum. *Ctnnb1*$^{\Delta i.enh}$
482 mice were generated in the Beijing Biocytogen. *H11*$^{i.enh}$ reporter mice were
483 generated in the Shanghai Model Organisms Center Inc. BAT-Gal mice were
484 provided by Dr. Jun-Lei Chang (Jackson Lab, stock number 005317). *Lgr5*-
485 EGFP-IRES-CreERT2 mice were gifts from Dr. Ye-Guang Chen (Jackson Lab,
486 stock number 008875). *APC*$^{Min/+}$ mice were gifts from Dr. Bo Zhong (Jackson
487 Lab, stock number 002020). The primer set forward 5′-atcctctgcatggtcaggtc-
488 3′/reverse 5′-cgtggcctgattcattcc-3′ was used for genotyping of BAT-Gal mice,
489 *H11*$^{i.enh}$ mice and *H11*$^{hi.enh}$ mice with a band size of 315 base pairs (bp). The
490 primer set forward 5′-gtcctgtccgtcactattatcctggc-3′/reverse5′-
491 ccactgccctgctaaagcattggt-3′/reverse 5′-tgattagttctccgggaagcccagt-3′ were
492 used for genotyping of *Ctnnb1*$^{\Delta i.enh}$ mice and band sizes for *Ctnnb1*$^{\Delta i.enh}$ mice
493 are 482 bp (wild-type allele) and 867 bp (ieCtnnb1 knockout allele). The primer
494 set forward *5′-atctcatggcaaacagacct-3′/reverse5′-tcacaaatcatctcgcaga-3′* was
495 used for genotyping of *APC*$^{Min/+}$ mice with a band size of 340 bp. The primer set

496 *forward 5′-ctgctctctgctcccagtct-3′/reverse5′-ataccccatccctttgagc-3′/reverse*
497 *5′-gaacttcagggtcagcttgc-3′* were used for genotyping of *Lgr5*-EGFP-IRES-
498 creERT2 mice and the band sizes for 386 bp (wild-type allele) and 119 bp
499 (mutant allele).
500
501 **Cell lines**
502 HEK293T cells were gifts from Dr. Hong-Bing Shu (Wuhan University). HCT116,
503 HCT-15 and HeLa cells were purchased from the China Center for Type Culture
504 Collection. HEK293T, HeLa and HCT116 cells were grown in DMEM (Gibco)
505 supplemented with 10% fetal bovine serum (FBS) (Life Technologies) and
506 1×penicillin/streptomycin (Gibco). HCT-15 cells were maintained in RPMI-1640
507 (Gibco) containing 10% FBS (Life Technologies) and 1×penicillin/streptomycin
508 (Gibco). For routine culturing, cells were dissociated using 0.25% trypsin
509 (Gibco).
510
511 **Tissue fixation and section**
512 Intestinal and tumor tissues were dissected and cleaned in pre-cooled
513 phosphate buffered saline (PBS) and immersed in 4% paraformaldehyde (PFA)
514 overnight at 4°C. For sectioning, intestines were embedded in Tissue-Tek®
515 O.C.T. Compound (SAKURA) and cut to 8 μm thickness with a cryostat (Leica
516 CM1950).
517
518 **CRISPR/dCas9-mediated transcription activation (CRISPRa) and**
519 **interference (CRISPRi) assay**
520 CRISPRa and CRISPRi assay were performed as previously described (**Wang**
521 **et al., 2022**). In brief, SgRNAs were designed using online tool
522 (https://zlab.bio/guide-design-resources) and were listed in **Table S2**. SgRNAs
523 were cloned into lenti sgRNA (MS2)_zeo backbone vector (Addgene, #61427).
524 For CRISPRi assays, pHR-SFFV-dCas9-BFP-KRAB (Addgene, #46911) is
525 used. For CRISPRa assays, lenti MS2-P65-HSF1_Hygro (Addgene, #61426)
526 and dCAS9-VP64_GFP (Addgene, #61422) were used. To obtain lentiviral
527 particles, HEK293T cells (5 × 10^6 cells per 10-cm dish) were transiently

transfected with 12 μg CRISPRa or CRISPRi constructs, 6 μg psPAX2 and 6 μg pMD2.G. The supernatant containing lentivirus particles was harvested at 72 hours after transfection and filtered through Millex-GP Filter Unit (0.45 μm pore size, Millipore). To obtain high virus titer, the supernatant was centrifuged at 10,000×*g* for 100 minutes and concentrate to 100 μl. On the day before infection, HCT-15 cells (2×10^5 cells per well) were inoculated in 12 well plates. 10 μl high titer viruses were added to each well. 72 hours after infection, cells were harvested for RT-qPCR analysis.

RNA isolation and cDNA synthesis

RNAiso Plus (TAKARA) is used for RNA isolation. 1 ml RNAiso Plus was added to DNase/RNase free EP tube to lyse tissues or cells, followed by adding one-fifth volume of chloroform to achieve phase separation. After vigorous shaking, centrifuge at 12,000×*g* for 15 minutes at 4°C. The upper aqueous phase was transferred to a new DNase/RNase free EP tube and equal volume of isopropanol was added to precipitate RNA. Precipitation was dissolved in DNase/RNase-free water. Complementary DNAs (cDNAs) were synthesized by HiScript® II Q RT SuperMix for qPCR kit (Vazyme; R222-01).

Real-time quantitative reverse transcription PCR (RT-qPCR)

cDNA was subjected to RT-qPCR using the SYBR Green assay with 2× SYBR Green qPCR master mix (Bimake). PCR reactions were performed on a CFX Connect Real-Time PCR Detection System (Bio-rad) under the following condition: 5 minutes at 95°C, 40 cycles at 95°C for 15 seconds, 60°C for 20 seconds. The relative transcript level of each gene was normalized to *Gapdh* (mice) or *ACTB* (human) and calculated according to the $2^{-\Delta\Delta Ct}$ method. All primers used are shown in the **Table S2**.

Isolation of murine intestinal crypt cells

Murine small intestines were harvested and cut open longitudinally. After 3 times wash in cold PBS with Penicillin (200 U/ml) + Streptomycin (200 μg/ml) (Invitrogen), small intestines were cut into 5 cm segments and incubated in pre-

560 cold PBS with 8 mM EDTA at 4°C for 2 hours. Then intestinal tissues were
561 transferred into a centrifuge tube filled with new cold PBS. Shake vigorously for
562 5 minutes and collect intestinal epithelial cells (villi plus crypts) from the
563 supernatant. Centrifuge the supernatant to collect all epithelial cells or pass
564 through 70 μm cell filter (Corning) to filter out villi. Crypts were spun down in a
565 centrifuge at 300×*g* for 5 minutes.

566

567 **Enriching *Lgr5*-EGFP$^+$ cells**

568 Crypts were collected from *Lgr5*-EGFP and *H11$^{i.enh}$*;*Lgr5*-EGFP mice, followed
569 by resuspension and single-cell digestion in DMEM containing 0.25% trypsin
570 (Gibco) at 37°C for 5 minutes. Disaggregated cells were passed through 40 μm
571 cell strainers (Corning). *Lgr5*-EGFP$^+$ and *Lgr5*-EGFP$^-$ cells were collected using
572 a BD Arial III cell sorter.

573

574 **X-Gal staining**

575 X-Gal staining is performed as described (**Wang et al., 2022**). In short, frozen
576 slides were placed in fixed buffer (0.2% PFA, 0.1 M PIPES buffer (pH 6.9), 2
577 mM MgCl2, 5 mM EGTA) for 10 minutes, followed by rinse for two times with
578 PBS containing 2 mM $MgCl_2$. Then slides were incubated with detergent
579 solution (0.1 M PBS (pH 7.3), 2 mM MgCl2, 0.01% sodium deoxycholate, 0.02%
580 Nonidet P-40) for 10 minutes. Slides were incubated with freshly prepared and
581 filtered X-Gal staining solution (0.1 M PBS (pH 7.3), 2 mM MgCl2, 0.01%
582 sodium-deoxycholate, 0.02% Nonidet P-40, 5 mM $K_3Fe(CN)_6$, 5 mM
583 $K_4Fe(CN)_6{\cdot}3H_2O$ and 1 mg/ml X-Gal) overnight in the dark at 37°C. For whole
584 gastrointestinal tissues, tissues were fixed in freshly prepared 4% PFA for 10
585 minutes, followed by rinse with detergent solution for 5 minutes by three times.
586 Tissues were incubated with freshly prepared and filtered X-Gal staining
587 solution at 37°C for a few hours.

588

589 **EdU pulse-labeling experiment**

590 Mice were intraperitoneally injected with EdU (10 mg/kg of body weight). After
591 4 hours, harvest the intestines for frozen sectioning. Staining was performed

592 using BeyoClick™ EdU Cell Promotion Kit (C0075S, Beyotime, China)
593 according to the manufacturer's manual.
594
595 **ChIP-qPCR assay**
596 Cells were cross-linked with 1% formaldehyde for 10 minutes at room
597 temperature and then quenched with 0.125 M glycine for 5 minutes and washed
598 twice with cold PBS. Cells were resuspended with 500 μl lysis buffer (50 mM
599 Tris-HCl, pH 8.0, 0.5% SDS, 5 mM EDTA) and subjected to sonication on ice
600 with an output power of 100 W, 12 minutes, 0.5 seconds on, 0.5 seconds off.
601 After centrifugation, 1% of the supernatant was taken out as input. The rest of
602 the sonicated lysates was diluted into 0.1% SDS and divided into several equal
603 parts. Immunoprecipitation was performed overnight at 4°C on a rotating wheel
604 with sheared chromatin, protein G agarose beads and indicated antibodies: 2
605 μg HNF4α (Abcam, ab181604), 2 μg p-S133-CREB1 (Abcam, ab32096), 2 μg
606 IgG antibody (ABclonal, AC005). The next day, beads were cleaned three times
607 with Wash Buffer I (20 mM Tris-HCl, pH 8.0; 1% Triton X-100; 2 mM EDTA; 150
608 mM NaCl; 0.1% SDS), Wash Buffer II (20 mM Tris-HCl, pH 8.0; 1% Triton X-
609 100; 2 mM EDTA; 500 mM NaCl; 0.1% SDS), Wash Buffer III (10 mM Tris-HCl,
610 pH 8.0; 1 mM EDTA; 0.25 M LiCl; 1% NP-40; 1% deoxycholate) and TE buffer.
611 Protein-DNA complexes were de-crosslinked in 120 μl elution buffer (0.1 M
612 $NaHCO_3$, 1% SDS, 20 μg/ml proteinase K) and shaken at 65°C overnight. DNA
613 purification kit (TIANGEN) was used to extract DNA fragments for qPCR.
614
615 **Luciferase reporter assay**
616 The luciferase reporter assay was performed as described previously (**Li et al.,**
617 **2017**). Briefly, the core region of ieCtnnb1, 5 regions of ieCTNNB1 and the
618 region containing the mutation site were respectively cloned into pGL3-
619 promoter vector (Promega). HEK293T, HeLa and HCT116 cells were
620 transfected with pGL3-promoter vector and the plasmids mentioned above.
621 *Renilla* basic vector was co-transfected as a control for normalization of
622 luciferase activity. After 48 hours of transfection, Promega Dual Glo test kit
623 (Promega, E1910) was used to measure luciferase activity according to

624 manufacturer's instructions.

625

626 **Immunohistochemical staining**

627 Frozen sections were dried at 37°C, fixed with 4% PFA for 10 minutes, and then
628 washed three times with PBS. Antigen retrieval was performed using citrate
629 buffer (pH 6, epitope retrieval solution) at 95°C for 20 minutes. Slides were then
630 placed in 3% H_2O_2 solution for a few hours to remove endogenous catalase.
631 After washing with PBS three times, slides were blocked with 10% normal goat
632 serum for 1 hour, then incubated with the following primary antibodies overnight
633 at 4°C: rabbit anti-α-defensin5 (Abcam, ab80515, 1:500), rabbit anti-Ki67
634 (Abcam, ab15580, 1:500), rabbit anti-β-catenin (Cell Signaling Technology,
635 8480T, 1:100), rabbit anti-Muc2 (Thermo Fisher Scientific, PA5-21329, 1:500).
636 The next day, slides were incubated with biotin labeled secondary antibodies
637 at room temperature for 1 hour. Then, slides were incubated with the avidin-
638 biotin-peroxidase complex (VECTASTAIN Elite ABC system, Vector Labs).
639 Finally, colorization was performed in the reaction solution (Tris-HCl (pH 7.2),
640 5 mg/ml 3,3'-diaminobenzidine, 0.075% H_2O_2).

641

642 **H&E staining**

643 H&E staining kit (Beyotime Biotech, C0105S) was used for experiments. Frozen
644 slides were dried at 65°C, then dripped with hematoxylin staining solution for 5
645 minutes. Excess staining solution was rinsed off with water. Slides were
646 immersed in distilled water for 5 minutes, then rinsed with 95% ethanol, and
647 stained with eosin solution for 30 seconds. Subsequently, slides were put into
648 anhydrous ethanol for 2 minutes, and cleared with xylene for 5 minutes. After
649 air dry, slides were sealed with neutral resin.

650

651 **Immunoblotting analysis**

652 Crypt cells were lysed by 1× SDS loading buffer at 95°C for 10 minutes. After
653 short centrifugation, the supernatants were loaded onto 10% SDS-
654 polyacrylamide gel electrophoresis gels. Then, proteins were transferred onto

655 polyvinylidene fluoride membrane (Millipore). Membranes were blocked with 10%
656 non-fat milk in tris-buffered saline containing 0.3% Tween 20 (TBST; pH 7.4)
657 for 1 hour at room temperature. Immunoblotting was carried out used primary
658 antibody: rabbit anti-β-catenin (Cell Signaling Technology, 8480T, 1:100);
659 mouse anti-GAPDH (ABclonal, AC001, 1:1000); rabbit anti-H3 (ABclonal,
660 A2348, 1:10,000). After three times of washing with TBST, the membrane was
661 incubated with anti-rabbit immunoglobulin G (IgG)–conjugated horseradish
662 peroxidase secondary for 1 hour at room temperature. Signals were detected
663 using the ECL substrate (Thermo Fisher Scientific).
664
665 **Alcian Blue PAS Staining**
666 Alcian Blue PAS Stain Kit (Abcam, ab245876) was used for experiments. all
667 materials and prepared reagents were equilibrated to room temperature and
668 gently agitated prior to use. Tissue sections were applied with acetic acid
669 solution (3%) for 2 minutes. Then alcian blue solution (pH 2.5) was applied for
670 15-20 minutes. Slides were rinsed with running tap water for 2 minutes followed
671 by 2 changes of distilled water. Periodic acid solution was applied to tissue
672 sections for 5 minutes. After slides were rinsed with two changes of distilled
673 water, Schiff's solution was applied to tissue sections for 10-20 minutes. Slides
674 were rinsed with warm running tap water for 2 minutes followed by 2 changes
675 of distilled water. Tissue sections were applied with hematoxylin for 2 minutes.
676 Sections were rinsed in running tap water for 2 minutes followed by 2 changes
677 of distilled water. Slides were dehydrated through graded alcohols and sealed
678 with synthetic resin.
679
680 **Cell Sorting**
681 Crypt single cells were prepared as described above. Cells were resuspended
682 using 1 ml PBS and stained with 5 μl anti-EpCAM-FITC (eBioScience, 11-5791-
683 82) at 4°C for 30 minutes. After washing with PBS three times, cells were
684 resuspended using 1 M FACS buffer (PBS with 1%BSA) containing 0.2 μg/ml
685 DAPI (BD Pharmingen, Cat. No. 564907). Cells were filtered with nylon
686 membrane with a 40 μm pore size. EpCAM positive cells were sorted and

687 collected based on fluorescence signals for subsequent single cell sequencing.
688 Flow cytometry data were acquired on a BD Arial III flow cytometer and
689 analyzed with FlowJo (version 10.6.2).
690
691 **Bulk RNA sequencing**
692 RNA-seq and data analyses were performed at Novogene Co., Ltd (Beijing,
693 China). Crypt cells or tumor tissues were harvested and total RNAs were
694 extracted. RNA integrity was assessed using the RNA Nano 6000 Assay Kit of
695 the Bioanalyzer 2100 system (Agilent Technologies, CA, USA). RNA-seq
696 library construction was performed as described previously (**Xu et al., 2021**).
697 Briefly, first strand cDNA was synthesized using random hexamer primer and
698 M-MuLV Reverse Transcriptase (RNase H-). Second strand cDNA synthesis
699 was subsequently performed using DNA Polymerase I and RNase H. Then, the
700 library fragments were purified with AMPure XP system (Beckman Coulter,
701 Beverly, USA). Then PCR was performed with Phusion High-Fidelity DNA
702 polymerase, Universal PCR primers and Index (X) Primer. At last, PCR
703 products were purified (AMPure XP system). The clustering of the index-coded
704 samples was performed on a cBot Cluster Generation System using TruSeq
705 PE Cluster Kit v3-cBot-HS (Illumia) according to the manufacturer's instructions.
706 After cluster generation, the library preparations were sequenced on an Illumina
707 Novaseq platform and 150 bp paired-end reads were generated.
708
709 **Bulk RNA-seq data processing**
710 For data analysis, raw data of fastq format were firstly processed through in-
711 house perl scripts. In this step, clean data were obtained by removing reads
712 containing adapter, reads containing ploy-N and low-quality reads from raw
713 data. Index of the reference genome was built using Hisat2 v2.0.5 and paired-
714 end clean reads were aligned to the reference genome using Hisat2 v2.0.5.
715 featureCounts v1.5.0-p3 was used to count reads numbers mapped to each
716 gene. Differential expression analysis of two groups was performed using the
717 DESeq2 R package (1.20.0). The resulting P-values were adjusted using the
718 Benjamini and Hochberg's approach for controlling the false discovery rate.

Genes with an adjusted P-value <0.05 found by DESeq2 were assigned as differentially expressed. Gene Ontology (GO) enrichment analysis of differentially expressed genes was implemented by the clusterProfiler R package, in which gene length bias was corrected. clusterProfiler R package was also used to test the statistical enrichment of differential expression genes in KEGG pathways. Local version of the GSEA analysis tool (http://www.broadinstitute.org/gsea/index.jsp), GO、KEGG、Reactome、DO and DisGeNET data sets were used for GSEA independently.

Single-Cell RNA sequencing and data analysis

ScRNA-seq and data analysis were performed at Novogene Co., Ltd (Beijing, China). The protoplast suspension was loaded into Chromium microfluidic chips with 30 chemistry (v2 or v3) and barcoded with a 10× Chromium Controller (10X Genomics). RNA from the barcoded cells was subsequently reverse-transcribed and sequencing libraries constructed with reagents from a Chromium Single Cell 30 v2 reagent kit (10X Genomics) according to the manufacturer's instructions. Sequencing was performed with Illumina HiSeq 2000 according to the manufacturer's instructions. For data analysis, we use FastQC to perform basic statistics on the quality of the raw reads. Raw reads were demultiplexed and mapped to the reference genome by 10X Genomics Cell Ranger pipeline using default parameters. All downstream single-cell analyses were performed using Cell Ranger and Seurat unless mentioned specifically. In brief, for each gene and each cell barcode (filtered by CellRanger), unique molecule identifiers were counted to construct digital expression matrices. Secondary filtration by Seurat: a gene with expression in more than 3 cells was considered as expressed, and each cell was required to have at least 200 expressed genes.

Hi-C data analysis

Hi-C data analysis completed by Frasergen Medicine Co., Ltd (Wuhan, China). Hi-C data of BALB/c mice large intestinal epithelial cells were provided by Dr. Gen Zheng(Zheng et al., 2023). The Hi-C data of SW480 cells was obtained

751 from deposited data(Orouji, 2022). According to the reported method, the
752 dynamic changes of TAD structures can be explored by calculating the relative
753 signal values of TAD boundaries. TAD boundaries that are common among
754 individuals and are not within the 2 Mb range of chromosomal ends were
755 included, followed by filtering out boundaries with interactions less than 10 in
756 the 2 Mb upstream and downstream regions. The ratio of the interaction
757 between the boundary and its 2 Mb upstream and downstream regions were
758 calculated using log2 to obtain the signal value of the TAD boundary, then the
759 minimum value was subtracted from it to finally obtain the distribution of the
760 relative signal value of each sample TAD boundary.
761
762 **ChIP-seq data analysis**
763 The human colorectal cancer patient RNA-seq FPKM files and ChIP-seq data
764 were from GEO dataset GSE156614 (**Q. L. Li et al., 2021**). All ChIP-seq raw
765 fastq data were removed of adaptor sequence. Cutadapt (version 1.16) was
766 used with the parameters -u 3 -u -10 -U 3 -U -10 -m 30. Cleaned reads were
767 aligned to the human reference genome (hg19) using bowtie2 (version 2.4.4)
768 with default settings. The CrossMap (0.6.5) package was used as a conversion
769 between different versions of the human genome (hg19 and hg38). We
770 calculated the normalized RPM (reads per million mapped reads) of ChIP-seq
771 signal at ieCTNNB1 and *CTNNB1* promoter. Briefly, reads aligned to the
772 specified region were calculated with bedtools multicov command. These reads
773 were normalized with RPM. RNA-seq data FPKM (Reads per kilobase per
774 million mapped reads) were converted to TPM (Transcript per Kilobase per
775 Million mapped reads) using R version 4.2.3.
776
777 **Knockdown experiments**
778 Target sequences for shRNAs were designed on the Merck Life Sciences
779 website (https://www.sigmaaldrich.cn) and were listed in **Table S2**.
780 Oligonucleotides for shRNAs were cloned into pLKO.1 vector (Addgene,
781 #21297). The day before transfection, HEK293T cells (2×10^5 cells per well)
782 were seeded in 12-well plates. pLKO.1 constructs, psPAX2 and pMD2.G were

783 co-transfected into HEK293T cells. After 72 hours, supernatant containing virus
784 particles was harvested and passed through Millex-GP Filter Unit (0.45 μm pore
785 size, Millipore). Viral particles were aliquoted and stored at -80°C. On the day
786 before infection, HCT-15 cells (2×10^5 cells per well) were seeded in 12-well
787 plates. 20 μl virus suspension were added to each well. After 72 hours, cells
788 were harvested for RT-qPCR to evalutate knockdown efficiency.
789

790 **Reference database**

791 ChIP-seq signals for H3K27ac, H3K4me3, H3K4me1, H3K36me3, and DNase
792 I hypersensitivity data of stomach, intestines, liver, and other tissues at different
793 stages were downloaded from the ENCODE (https://www.encodeproject.org/)
794 and their identifiers are listed in **Table S1**. In addition, ChIP-seq data for listed
795 transcription factors of cells or tissues were obtained from Cistrome Data
796 Browser (http://cistrome.org). Expressions of *HNF4A* and *CREB1* in human
797 colon (COAD) and rectal (READ) cancers were obtained from GEPIA
798 (gepia.cancer-pku.cn).
799

800 **eQTL analysis**

801 The GTEX database (https://www.gtexportal.org/home/) was used to search
802 SNPs at *CTNNB1* and the 1 MB upstream and downstream region, followed by
803 eQTL analysis. A variant, rs115981379 (C>T), was identified inside *CTNNB1*.
804 The expression levels of *CTNNB1* in 428 C/C type and 37 C/T type esophagus
805 samples, and 343 C/C type and 25 C/T type transverse colon samples were
806 also obtained in the GTEX database.
807

808 **Analyses of HNF4α and CREB1 binding motifs**

809 The JASPAR database (https://jaspar.elixir.no/) was used to analyze binding
810 motifs of HNF4α and CREB1 at ieCtnnb1/ieCTNNB1 and *Ctnnb1/CTNNB1*
811 promoter. Results are listed in **Table S3**.
812

813 **Nuclear-cytoplasmic separation**

814 Nuclear and cytoplasmic protein extraction kit (Beyotime Biotech, P0027) was
815 used for experiments. Small intestinal crypts were collected from wild-type and
816 *Ctnnb1*$^{\Delta i.enh}$ mice as described above. According to manufacturer's instructions,
817 20 μl cell precipitation was resuspended in 200 μl cytoplasmic protein extraction
818 reagent A with 1 mM PMSF. After placing on ice for 15 minutes, 10 μl
819 cytoplasmic protein extraction reagent B was added. After vigorous vortex,
820 solutions were centrifuged at 12,000×*g* for 5 minutes at 4°C. The supernatant
821 was collected as the extracted cytoplasmic protein. The precipitate was
822 resuspended with 50 μl nuclear protein extraction reagent with 1 mM PMSF.
823 Solutions were placed on ice and vortex vigorously every 2 minutes for a total
824 of 30 minutes. After centrifuging at 12,000×*g* for 10 minutes at 4°C, the
825 supernatant was collected as the extracted nuclear protein.
826
827 **Statistics**
828 All experiments reported in this study were repeated at least three independent
829 times. *In vivo* analyses were conducted with at least three animals per condition.
830 The number of animals in each experiment is depicted in Figure legends. The
831 signal intensity of tumor stain region was generated using ImageJ software
832 (version 6.0.0.260) as described previously (**Wang et al., 2021**). GraphPad
833 Prism (version 8.0.2) was used to determine statistical significance. Unpaired
834 two-tailed Student's t-test were used for analysis between two groups of equal
835 variances by *F*-tests. When the *F*-test of equal variance failed, the Welch *t*-tests
836 were used. Data comparison of three or more groups with control groups were
837 analyzed using one-way ANOVA followed by Dunnett's multiple comparison
838 test. Data comparison of three or more groups among each other were
839 analyzed using one-way ANOVA followed by Tukey's multiple comparison test.
840 The exact *P* values were reported in each figure or indicated as ****, $P < 0.0001$;
841 ***, $P < 0.001$; **, $P < 0.01$; *, $P < 0.05$, ns = not significant.
842
843 **Data and code availability**
844 The GEO accession number for the bulk RNA-seq and scRNA-seq data

reported in this paper is GSE233979. RNA-seq data of mouse small intestinal crypt and colon tumor have been deposited at GEO: GSE233977. ScRNA-seq data of mouse small intestinal crypt cells in this study have been deposited at GEO: GSE233978. All data are publicly available as of the date of publication. Custom codes were described in detail at methods part. Any additional information required to analyze the data in this paper is available from authors upon reasonable request.

References

Andreu, P., Peignon, G., Slomianny, C., Taketo, M. M., Colnot, S., Robine, S., Lamarque, D., Laurent-Puig, P., Perret, C., & Romagnolo, B. 2008. A genetic study of the role of the Wnt/beta-catenin signalling in Paneth cell differentiation. *Dev Biol, **324***, 288-296. https://doi.org/10.1016/j.ydbio.2008.09.027

Ayyaz, A., Kumar, S., Sangiorgi, B., Ghoshal, B., Gosio, J., Ouladan, S., Fink, M., Barutcu, S., Trcka, D., Shen, J., Chan, K., Wrana, J. L., & Gregorieff, A. 2019. Single-cell transcriptomes of the regenerating intestine reveal a revival stem cell. *Nature, **569***, 121-125. https://doi.org/10.1038/s41586-019-1154-y

Bakker, E. R., Hoekstra, E., Franken, P. F., Helvensteijn, W., van Deurzen, C. H., van Veelen, W., Kuipers, E. J., & Smits, R. 2013. beta-Catenin signaling dosage dictates tissue-specific tumor predisposition in Apc-driven cancer. *Oncogene, **32***, 4579-4585. https://doi.org/10.1038/onc.2012.449

Barker, N., van Es, J. H., Kuipers, J., Kujala, P., van den Born, M., Cozijnsen, M., Haegebarth, A., Korving, J., Begthel, H., Peters, P. J., & Clevers, H. 2007. Identification of stem cells in small intestine and colon by marker gene Lgr5. *Nature, **449***, 1003-1007. https://doi.org/10.1038/nature06196

Barreto, E. B. L., Rattes, I. C., da Costa, A. V., & Gama, P. 2022. Paneth cells and their multiple functions. *Cell Biol Int, **46***, 701-710. https://doi.org/10.1002/cbin.11764

Beumer, J., & Clevers, H. 2016. Regulation and plasticity of intestinal stem cells during homeostasis and regeneration. *Development, **143***, 3639-3649. https://doi.org/10.1242/dev.133132

Beumer, J., & Clevers, H. 2020. Cell fate specification and differentiation in the adult mammalian intestine. *Nature Reviews Molecular Cell Biology, **22***, 39-53. https://doi.org/10.1038/s41580-020-0278-0

Carlezon, W. A., Jr., Duman, R. S., & Nestler, E. J. 2005. The many faces of CREB. *Trends Neurosci, **28***, 436-445. https://doi.org/10.1016/j.tins.2005.06.005

Cattin, A. L., Le Beyec, J., Barreau, F., Saint-Just, S., Houllier, A., Gonzalez, F. J., Robine, S., Pincon-Raymond, M., Cardot, P., Lacasa, M., & Ribeiro, A. 2009. Hepatocyte nuclear factor 4alpha, a key factor for homeostasis, cell architecture, and barrier function of the adult intestinal epithelium. *Mol Cell Biol, **29***, 6294-6308. https://doi.org/10.1128/MCB.00939-09

885 Cheng, X., Xu, X., Chen, D., Zhao, F., & Wang, W. 2019. Therapeutic potential of targeting
886 the Wnt/beta-catenin signaling pathway in colorectal cancer. *Biomed*
887 *Pharmacother,* ***110***, 473-481. https://doi.org/10.1016/j.biopha.2018.11.082
888 Chin, A. M., Hill, D. R., Aurora, M., & Spence, J. R. 2017. Morphogenesis and maturation
889 of the embryonic and postnatal intestine. *Semin Cell Dev Biol,* ***66***, 81-93.
890 https://doi.org/10.1016/j.semcdb.2017.01.011
891 Clevers, H. 2006. Wnt/beta-catenin signaling in development and disease. *Cell,* ***127***, 469-
892 480. https://doi.org/10.1016/j.cell.2006.10.018
893 Clevers, H. 2013. The intestinal crypt, a prototype stem cell compartment. *Cell,* ***154***, 274-
894 284. https://doi.org/10.1016/j.cell.2013.07.004
895 Clevers, H., Loh, K. M., & Nusse, R. 2014. Stem cell signaling. An integral program for
896 tissue renewal and regeneration: Wnt signaling and stem cell control. *Science,* ***346***,
897 1248012. https://doi.org/10.1126/science.1248012
898 Clevers, H., & Nusse, R. 2012. Wnt/beta-catenin signaling and disease. *Cell,* ***149***, 1192-
899 1205. https://doi.org/10.1016/j.cell.2012.05.012
900 Degirmenci, B., Valenta, T., Dimitrieva, S., Hausmann, G., & Basler, K. 2018. GLI1-
901 expressing mesenchymal cells form the essential Wnt-secreting niche for colon
902 stem cells. *Nature,* ***558***, 449-453. https://doi.org/10.1038/s41586-018-0190-3
903 Durand, A., Donahue, B., Peignon, G., Letourneur, F., Cagnard, N., Slomianny, C., Perret,
904 C., Shroyer, N. F., & Romagnolo, B. 2012. Functional intestinal stem cells after
905 Paneth cell ablation induced by the loss of transcription factor Math1 (Atoh1).
906 *Proceedings of the National Academy of Sciences,* ***109***, 8965-8970.
907 https://doi.org/10.1073/pnas.1201652109
908 Garabedian, E. M., Roberts, L. J. J., McNevin, M. S., & Gordon, J. I. 1997. Examining the
909 Role of Paneth Cells in the Small Intestine by Lineage Ablation in Transgenic Mice.
910 *Journal of Biological Chemistry,* ***272***, 23729-23740.
911 https://doi.org/10.1074/jbc.272.38.23729
912 Garrison, W. D., Battle, M. A., Yang, C., Kaestner, K. H., Sladek, F. M., & Duncan, S. A.
913 2006. Hepatocyte nuclear factor 4alpha is essential for embryonic development of
914 the mouse colon. *Gastroenterology,* ***130***, 1207-1220.
915 https://doi.org/10.1053/j.gastro.2006.01.003
916 Gribble, F. M., & Reimann, F. 2019. Function and mechanisms of enteroendocrine cells
917 and gut hormones in metabolism. *Nature Reviews Endocrinology,* ***15***, 226-237.
918 https://doi.org/10.1038/s41574-019-0168-8
919 Gustafsson, J. K., & Johansson, M. E. V. 2022. The role of goblet cells and mucus in
920 intestinal homeostasis. *Nature Reviews Gastroenterology & Hepatology,* ***19***, 785-
921 803. https://doi.org/10.1038/s41575-022-00675-x
922 Haber, A. L., Biton, M., Rogel, N., Herbst, R. H., Shekhar, K., Smillie, C., Burgin, G.,
923 Delorey, T. M., Howitt, M. R., Katz, Y., Tirosh, I., Beyaz, S., Dionne, D., Zhang, M.,
924 Raychowdhury, R., Garrett, W. S., Rozenblatt-Rosen, O., Shi, H. N., Yilmaz, O.,
925 Xavier, R. J., & Regev, A. 2017. A single-cell survey of the small intestinal
926 epithelium. *Nature,* ***551***, 333-339. https://doi.org/10.1038/nature24489
927 Hamdan, F. H., & Johnsen, S. A. 2019. Perturbing Enhancer Activity in Cancer Therapy.
928 *Cancers (Basel),* ***11***. https://doi.org/10.3390/cancers11050634

929 Huels, D. J., Bruens, L., Hodder, M. C., Cammareri, P., Campbell, A. D., Ridgway, R. A.,
930 Gay, D. M., Solar-Abboud, M., Faller, W. J., Nixon, C., Zeiger, L. B., McLaughlin,
931 M. E., Morrissey, E., Winton, D. J., Snippert, H. J., van Rheenen, J., & Sansom, O.
932 J. 2018. Wnt ligands influence tumour initiation by controlling the number of
933 intestinal stem cells. *Nature Communications, **9***. https://doi.org/10.1038/s41467-
934 018-03426-2
935 Jindal, G. A., & Farley, E. K. 2021. Enhancer grammar in development, evolution, and
936 disease: dependencies and interplay. *Dev Cell, **56***, 575-587.
937 https://doi.org/10.1016/j.devcel.2021.02.016
938 Kim, T.-H., Escudero, S., & Shivdasani, R. A. 2012. Intact function of Lgr5 receptor-
939 expressing intestinal stem cells in the absence of Paneth cells. *Proceedings of the*
940 *National Academy of Sciences, **109***, 3932-3937.
941 https://doi.org/10.1073/pnas.1113890109
942 Krausova, M., & Korinek, V. 2014. Wnt signaling in adult intestinal stem cells and cancer.
943 *Cell Signal, **26***, 570-579. https://doi.org/10.1016/j.cellsig.2013.11.032
944 Kurokawa, K., Hayakawa, Y., & Koike, K. 2020. Plasticity of Intestinal Epithelium: Stem
945 Cell Niches and Regulatory Signals. *Int J Mol Sci, **22***.
946 https://doi.org/10.3390/ijms22010357
947 Kvon, E. Z., Waymack, R., Gad, M., & Wunderlich, Z. 2021. Enhancer redundancy in
948 development and disease. *Nat Rev Genet, **22***, 324-336.
949 https://doi.org/10.1038/s41576-020-00311-x
950 Kvon, E. Z., Zhu, Y., Kelman, G., Novak, C. S., Plajzer-Frick, I., Kato, M., Garvin, T. H.,
951 Pham, Q., Harrington, A. N., Hunter, R. D., Godoy, J., Meky, E. M., Akiyama, J. A.,
952 Afzal, V., Tran, S., Escande, F., Gilbert-Dussardier, B., Jean-Marcais, N.,
953 Hudaiberdiev, S., Ovcharenko, I., Dobbs, M. B., Gurnett, C. A., Manouvrier-Hanu,
954 S., Petit, F., Visel, A., Dickel, D. E., & Pennacchio, L. A. 2020. Comprehensive In
955 Vivo Interrogation Reveals Phenotypic Impact of Human Enhancer Variants. *Cell,*
956 ***180***, 1262-1271 e1215. https://doi.org/10.1016/j.cell.2020.02.031
957 Li, J., Ma, X., Chakravarti, D., Shalapour, S., & DePinho, R. A. 2021. Genetic and biological
958 hallmarks of colorectal cancer. *GENES & DEVELOPMENT, **35***, 787-820.
959 https://doi.org/10.1101/gad.348226
960 Li, Q. L., Lin, X., Yu, Y. L., Chen, L., Hu, Q. X., Chen, M., Cao, N., Zhao, C., Wang, C. Y.,
961 Huang, C. W., Li, L. Y., Ye, M., & Wu, M. 2021. Genome-wide profiling in colorectal
962 cancer identifies PHF19 and TBC1D16 as oncogenic super enhancers. *Nat*
963 *Commun, **12***, 6407. https://doi.org/10.1038/s41467-021-26600-5
964 Li, Y., Wang, W., Wang, F., Wu, Q., Li, W., Zhong, X., Tian, K., Zeng, T., Gao, L., Liu, Y.,
965 Li, S., Jiang, X., Du, G., & Zhou, Y. 2017. Paired related homeobox 1 transactivates
966 dopamine D2 receptor to maintain propagation and tumorigenicity of glioma-
967 initiating cells. *Journal of Molecular Cell Biology, **9***, 302-314.
968 https://doi.org/10.1093/jmcb/mjx017
969 Lueschow, S. R., & McElroy, S. J. 2020. The Paneth Cell: The Curator and Defender of
970 the Immature Small Intestine. *Front Immunol, **11***, 587.
971 https://doi.org/10.3389/fimmu.2020.00587
972 Luis, Tiago C., Naber, Brigitta A. E., Roozen, Paul P. C., Brugman, Martijn H., de Haas,

Edwin F. E., Ghazvini, M., Fibbe, Willem E., van Dongen, Jacques J. M., Fodde, R., & Staal, Frank J. T. 2011. Canonical Wnt Signaling Regulates Hematopoiesis in a Dosage-Dependent Fashion. *Cell Stem Cell,* ***9***, 345-356. https://doi.org/10.1016/j.stem.2011.07.017

Mah, A. T., Yan, K. S., & Kuo, C. J. 2016. Wnt pathway regulation of intestinal stem cells. *J Physiol,* ***594***, 4837-4847. https://doi.org/10.1113/JP271754

Metcalfe, C., Kljavin, N. M., Ybarra, R., & de Sauvage, F. J. 2014. Lgr5+ stem cells are indispensable for radiation-induced intestinal regeneration. *Cell Stem Cell,* ***14***, 149-159. https://doi.org/10.1016/j.stem.2013.11.008

Nakamura, T., Tsuchiya, K., & Watanabe, M. 2007. Crosstalk between Wnt and Notch signaling in intestinal epithelial cell fate decision. *J Gastroenterol,* ***42***, 705-710. https://doi.org/10.1007/s00535-007-2087-z

Nalapareddy, K., Nattamai, K. J., Kumar, R. S., Karns, R., Wikenheiser-Brokamp, K. A., Sampson, L. L., Mahe, M. M., Sundaram, N., Yacyshyn, M.-B., Yacyshyn, B., Helmrath, M. A., Zheng, Y., & Geiger, H. 2017. Canonical Wnt Signaling Ameliorates Aging of Intestinal Stem Cells. *Cell Reports,* ***18***, 2608-2621. https://doi.org/10.1016/j.celrep.2017.02.056

Noah, T. K., Donahue, B., & Shroyer, N. F. 2011. Intestinal development and differentiation. *Exp Cell Res,* ***317***, 2702-2710. https://doi.org/10.1016/j.yexcr.2011.09.006

Nusse, R., & Clevers, H. 2017. Wnt/beta-Catenin Signaling, Disease, and Emerging Therapeutic Modalities. *Cell,* ***169***, 985-999. https://doi.org/10.1016/j.cell.2017.05.016

Orouji, E., Raman, A. T., Singh, A. K., Sorokin, A., Arslan, E., Ghosh, A. K., Schulz, J., Terranova, C., Jiang, S., Tang, M., Maitituoheti, M., Callahan, S. C., Barrodia, P., Tomczak, K., Jiang, Y., Jiang, Z., Davis, J. S., Ghosh, S., Lee, H. M., Reyes-Uribe, L., … Rai, K. 2022. Chromatin state dynamics confers specific therapeutic strategies in enhancer subtypes of colorectal cancer. *Gut,* ***71(5)***, 938–949. https://doi.org/ https://doi.org/10.1136/gutjnl-2020-322835

Pachano, T., Haro, E., & Rada-Iglesias, A. 2022. Enhancer-gene specificity in development and disease. *Development,* ***149***. https://doi.org/10.1242/dev.186536

Pentinmikko, N., Iqbal, S., Mana, M., Andersson, S., Cognetta, A. B., Suciu, R. M., Roper, J., Luopajärvi, K., Markelin, E., Gopalakrishnan, S., Smolander, O.-P., Naranjo, S., Saarinen, T., Juuti, A., Pietiläinen, K., Auvinen, P., Ristimäki, A., Gupta, N., Tammela, T., Jacks, T., Sabatini, D. M., Cravatt, B. F., Yilmaz, Ö. H., & Katajisto, P. 2019. Notum produced by Paneth cells attenuates regeneration of aged intestinal epithelium. *Nature,* ***571***, 398-402. https://doi.org/10.1038/s41586-019-1383-0

Pinto, D., & Clevers, H. 2005. Wnt control of stem cells and differentiation in the intestinal epithelium. *Exp Cell Res,* ***306***, 357-363. https://doi.org/10.1016/j.yexcr.2005.02.022

Pinto, D., Gregorieff, A., Begthel, H., & Clevers, H. 2003. Canonical Wnt signals are essential for homeostasis of the intestinal epithelium. *Genes Dev,* ***17***, 1709-1713. https://doi.org/10.1101/gad.267103

Ramadan, R., van Driel, M. S., Vermeulen, L., & van Neerven, S. M. 2022. Intestinal stem

cell dynamics in homeostasis and cancer. *Trends Cancer,* ***8***, 416-425. https://doi.org/10.1016/j.trecan.2022.01.011

Rim, E. Y., Clevers, H., & Nusse, R. 2022. The Wnt Pathway: From Signaling Mechanisms to Synthetic Modulators. *Annu Rev Biochem,* ***91***, 571-598. https://doi.org/10.1146/annurev-biochem-040320-103615

Sato, T., van Es, J. H., Snippert, H. J., Stange, D. E., Vries, R. G., van den Born, M., Barker, N., Shroyer, N. F., van de Wetering, M., & Clevers, H. 2011. Paneth cells constitute the niche for Lgr5 stem cells in intestinal crypts. *Nature,* ***469***, 415-418. https://doi.org/10.1038/nature09637

Schneider, C., O'Leary, C. E., & Locksley, R. M. 2019. Regulation of immune responses by tuft cells. *Nature Reviews Immunology,* ***19***, 584-593. https://doi.org/10.1038/s41577-019-0176-x

Sengupta, S., & George, R. E. 2017. Super-Enhancer-Driven Transcriptional Dependencies in Cancer. *Trends Cancer,* ***3***, 269-281. https://doi.org/10.1016/j.trecan.2017.03.006

Shoshkes-Carmel, M., Wang, Y. J., Wangensteen, K. J., Tóth, B., Kondo, A., Massasa, E. E., Itzkovitz, S., & Kaestner, K. H. 2018. Subepithelial telocytes are an important source of Wnts that supports intestinal crypts. *Nature,* ***557***, 242-246. https://doi.org/10.1038/s41586-018-0084-4

Silvia Maretto, M. C., Sirio Dupont, Paola Braghetta, Vania Broccoli, A. Bassim Hassan, Dino Volpin, Giorgio M. Bressan, and Stefano Piccolo. 2003. Mapping Wnt/β-catenin signaling during mouse development and in colorectal tumors. *PNAS*.

Snoeck, V., Goddeeris, B., & Cox, E. 2005. The role of enterocytes in the intestinal barrier function and antigen uptake. *Microbes and Infection,* ***7***, 997-1004. https://doi.org/10.1016/j.micinf.2005.04.003

Su, L. K., Kinzler, K. W., Vogelstein, B., Preisinger, A. C., Moser, A. R., Luongo, C., Gould, K. A., & Dove, W. F. 1992. Multiple intestinal neoplasia caused by a mutation in the murine homolog of the APC gene. *Science,* ***256***, 668-670. https://doi.org/10.1126/science.1350108

Terrin, L., Agostini, M., Ruvoletto, M., Martini, A., Pucciarelli, S., Bedin, C., Nitti, D., & Pontisso, P. 2017. SerpinB3 upregulates the Cyclooxygenase-2 / beta-Catenin positive loop in colorectal cancer. *Oncotarget,* ***8***, 15732-15743. https://doi.org/10.18632/oncotarget.14997

Tian, H., Biehs, B., Warming, S., Leong, K. G., Rangell, L., Klein, O. D., & de Sauvage, F. J. 2011. A reserve stem cell population in small intestine renders Lgr5-positive cells dispensable. *Nature,* ***478***, 255-259. https://doi.org/10.1038/nature10408

van der Flier, L. G., & Clevers, H. 2009. Stem cells, self-renewal, and differentiation in the intestinal epithelium. *Annu Rev Physiol,* ***71***, 241-260. https://doi.org/10.1146/annurev.physiol.010908.163145

van Es, J. H., Jay, P., Gregorieff, A., van Gijn, M. E., Jonkheer, S., Hatzis, P., Thiele, A., van den Born, M., Begthel, H., Brabletz, T., Taketo, M. M., & Clevers, H. 2005. Wnt signalling induces maturation of Paneth cells in intestinal crypts. *Nat Cell Biol,* ***7***, 381-386. https://doi.org/10.1038/ncb1240

van Es, J. H., Sato, T., van de Wetering, M., Lyubimova, A., Yee Nee, A. N., Gregorieff, A.,

Sasaki, N., Zeinstra, L., van den Born, M., Korving, J., Martens, A. C. M., Barker, N., van Oudenaarden, A., & Clevers, H. 2012. Dll1+ secretory progenitor cells revert to stem cells upon crypt damage. *Nat Cell Biol, **14***, 1099-1104. https://doi.org/10.1038/ncb2581

Wang, A., Wang, J., Tian, K., Huo, D., Ye, H., Li, S., Zhao, C., Zhang, B., Zheng, Y., Xu, L., Hua, X., Wang, K., Wu, Q. F., Wu, X., Zeng, T., Liu, Y., & Zhou, Y. 2021. An epigenetic circuit controls neurogenic programs during neocortex development. *Development, **148***. https://doi.org/10.1242/dev.199772

Wang, J., Wang, A., Tian, K., Hua, X., Zhang, B., Zheng, Y., Kong, X., Li, W., Xu, L., Wang, J., Li, Z., Liu, Y., & Zhou, Y. 2022. A Ctnnb1 enhancer regulates neocortical neurogenesis by controlling the abundance of intermediate progenitors. *Cell Discov, **8***, 74. https://doi.org/10.1038/s41421-022-00421-2

Wong, E. S., Zheng, D., Tan, S. Z., Bower, N. L., Garside, V., Vanwalleghem, G., Gaiti, F., Scott, E., Hogan, B. M., Kikuchi, K., McGlinn, E., Francois, M., & Degnan, B. M. 2020. Deep conservation of the enhancer regulatory code in animals. *Science, **370***. https://doi.org/10.1126/science.aax8137

Xu, L., Zheng, Y., Li, X., Wang, A., Huo, D., Li, Q., Wang, S., Luo, Z., Liu, Y., Xu, F., Wu, X., Wu, M., & Zhou, Y. 2021. Abnormal neocortex arealization and Sotos-like syndrome–associated behavior in Setd2 mutant mice. *Science Advances, **7***, 1180. https://doi.org/10.1126/sciadv.aba1180

Yan, K. S., Chia, L. A., Li, X., Ootani, A., Su, J., Lee, J. Y., Su, N., Luo, Y., Heilshorn, S. C., Amieva, M. R., Sangiorgi, E., Capecchi, M. R., & Kuo, C. J. 2012. The intestinal stem cell markers Bmi1 and Lgr5 identify two functionally distinct populations. *Proc Natl Acad Sci U S A, **109***, 466-471. https://doi.org/10.1073/pnas.1118857109

Zabidi, M. A., & Stark, A. 2016. Regulatory Enhancer-Core-Promoter Communication via Transcription Factors and Cofactors. *Trends Genet, **32***, 801-814. https://doi.org/10.1016/j.tig.2016.10.003

Zhang, Y., & Wang, X. 2020. Targeting the Wnt/beta-catenin signaling pathway in cancer. *J Hematol Oncol, **13***, 165. https://doi.org/10.1186/s13045-020-00990-3

Zhao, H., Ming, T., Tang, S., Ren, S., Yang, H., Liu, M., Tao, Q., & Xu, H. 2022. Wnt signaling in colorectal cancer: pathogenic role and therapeutic target. *Mol Cancer, **21***, 144. https://doi.org/10.1186/s12943-022-01616-7

Zheng, G., Pang, S., Wang, J., Wang, F., Wang, Q., Yang, L., Ji, M., Xie, D., Zhu, S., Chen, Y., Zhou, Y., Higgins, G. A., Wiley, J. W., Hou, X., & Lin, R. 2023. Glucocorticoid receptor-mediated Nr1d1 chromatin circadian misalignment in stress-induced irritable bowel syndrome. *iScience, **26***, 107137. https://doi.org/10.1016/j.isci.2023.107137

Zhu, Y., & Li, X. 2023. Advances of Wnt Signalling Pathway in Colorectal Cancer. *Cells, **12***. https://doi.org/10.3390/cells12030447

Acknowledgments

We thank Dr. Yeguang Chen for providing the *Lgr5*-EGFP-IRES-CreERT2 mice.

We thank the Core Facility and the Animal Facility of Medical Research Institute of Wuhan University for technical support. We thank all Zhou lab members for critical reading of the manuscript. Y. Zhou was supported by grants from National Key R&D Program of China (2022YFA0806603 and 2018YFA0800700), National Natural Science Foundation of China (32270876 and 31970770), and the Fundamental Research Funds for the Central Universities (2042022dx0003 and 2042023kf0234). Y.L. was supported by grants from National Key R&D Program of China (2018YFA0800700 and 2022YFA0806603), National Natural Science Foundation of China (31970676), and Hubei Natural Science Foundation (2022CFB128).

Author contributions

Y.Z. conceived and designed the study; X.H. and J.W. performed experiments and analyzed data; C.Z. assisted with processing ChIP-seq data; J.T. and X.P. retrieved and analyzed eQTL data. M.Y. and M.W. provided RNA-seq and ChIP-seq data of colorectal cancer samples; G.Z. provided Hi-C data; Y.Z. and X.H. wrote the paper. Y.Z. and Y.L. provided funding and supervised the study. All authors discussed results and commented to the manuscript.

Competing interests

The authors claimed that they have no competing interests.

Figures

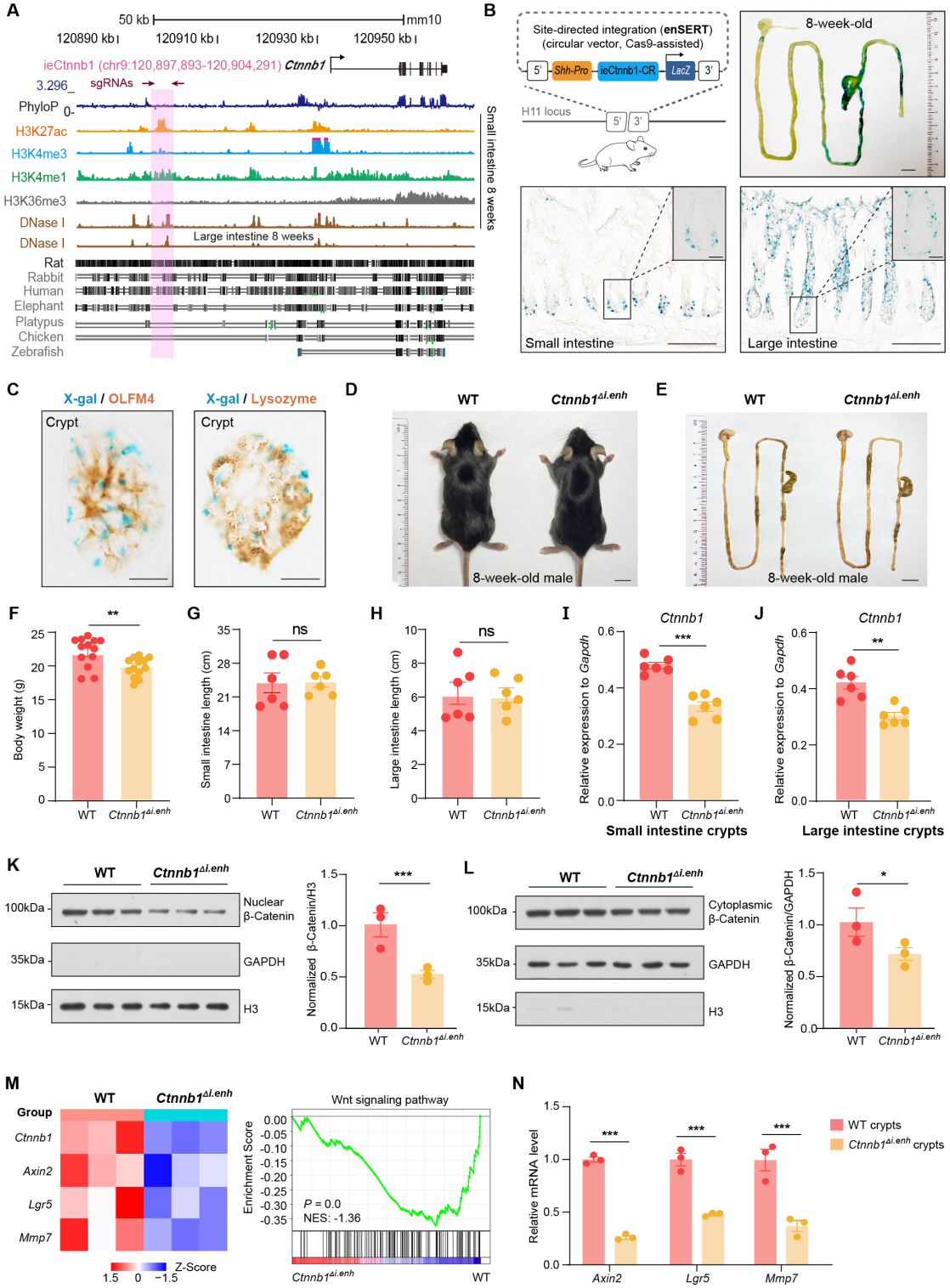

Figure 1

Figure 1. ieCtnnb1 is an intestinal enhancer of *Ctnnb1*. (A) Schematic representation of the upstream region of mouse *Ctnnb1* gene and the location of ieCtnnb1 (6,399 bp, pink shading), which is marked by H3K27ac and

1130 H3K4me1 peaks, and DNase I hypersensitivity in small intestine and large
1131 intestine of 8-week-old mice. Data were obtained from ENCODE. Locations of
1132 single-guide RNAs (sgRNAs) for generating ieCtnnb1 knockout mice were
1133 marked. (B) Top left: a schematic illustration showing that the knock-in reporter
1134 construct carries the *Shh* promoter, ieCtnnb1 core region sequences (2,153 bp)
1135 and the *LacZ* reporter gene. Top right: X-Gal staining (blue) of the
1136 gastrointestinal (GI) tract of an 8-week-old $H11^{i.enh}$ mouse. Bottom: X-Gal
1137 staining (blue) of the small intestine (left) and colon (right) of an 8-week-old
1138 $H11^{i.enh}$ mouse. Boxed areas were enlarged at top-right corners. (C)
1139 Representative images of small intestinal crypts co-labelled by X-gal with
1140 OLFM4 (left), and X-gal with Lysozyme (right). (D-E) Representative images of
1141 whole body (d) and GIs (e) of 8-week-old male wildtype (WT) and $Ctnnb1^{\Delta i.enh}$
1142 mice. (F) Comparison of the body weight of 8-week-old male WT (n = 13) and
1143 $Ctnnb1^{\Delta i.enh}$ (n = 13) mice. (G-H) Measurements of small (G) and large (H)
1144 intestine length of 8-week-old male WT (n = 6) and $Ctnnb1^{\Delta i.enh}$ (n = 6) mice. (I-
1145 J) Relative mRNA levels of *Ctnnb1* in small (I) and large (J) intestinal crypts of
1146 WT (n = 6) and $Ctnnb1^{\Delta i.enh}$ (n = 6) mice. (K-L) Left: immunoblotting of nuclear
1147 (K) and cytoplasmic (L) β-Catenin, GAPDH and H3 of small intestinal crypts of
1148 WT (n = 3) and $Ctnnb1^{\Delta i.enh}$ (n = 3) mice. Right: histograms showing protein
1149 levels of β-Catenin normalized to H3 (K) or GAPDH (L) levels. Values of WT
1150 were set as '1'. (M) Heat map of indicated Wnt target genes and GSEA analysis
1151 of Wnt signaling pathway according to transcriptome profiles of small intestinal
1152 crypts of WT (n = 3) and $Ctnnb1^{\Delta i.enh}$ (n = 3) mice. (N) RT-qPCR showing
1153 relative mRNA levels of indicated Wnt target genes (*Axin2, Lgr5* and *Mmp7*) in
1154 small intestinal crypts of WT (n = 3) and $Ctnnb1^{\Delta i.enh}$ (n = 3) mice. Scale bars,
1155 1 cm (B, top; D and E), 100 μm (B, bottom), 10 μm (B, magnified views; C).
1156 Quantification data are shown as means ± SEM, statistical significance was
1157 determined using an unpaired two-tailed Student's *t*-test (F-L). Quantification
1158 data are shown means ± SD, statistical significance was determined using

1159 Multiple *t*-tests - one per row (N). *$P < 0.05$, **$P < 0.01$, ***$P < 0.001$, and ****P

1160 < 0.0001. ns, not significant. NES: Normalized Enrichment Score.

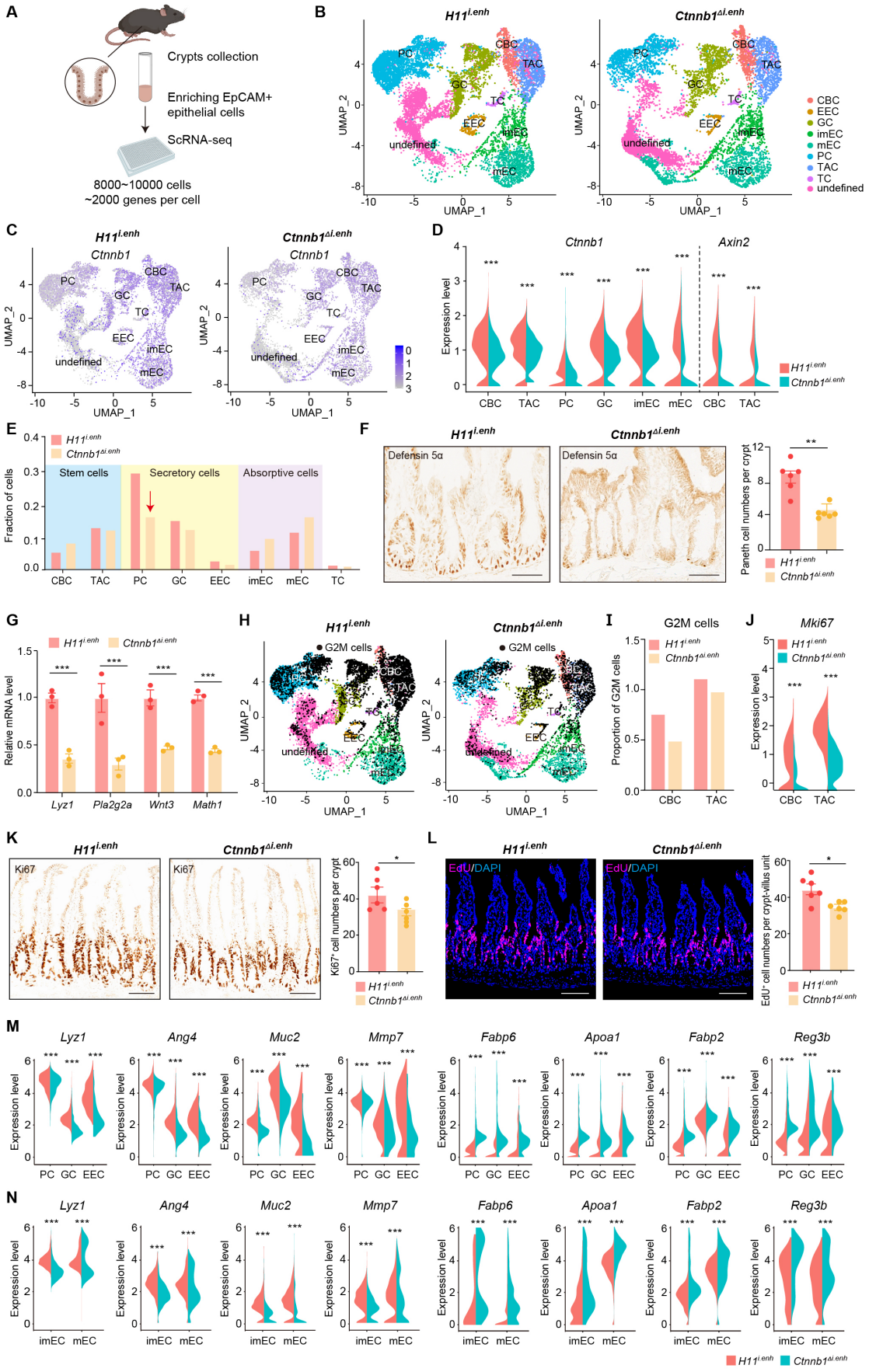
A
Crypts collection
Enriching EpCAM+ epithelial cells
ScRNA-seq
8000~10000 cells
~2000 genes per cell
B
H11i.enh
Ctnnb1Δi.enh
CBC
EEC
GC
imEC
mEC
PC
TAC
TC
undefined
UMAP_1
UMAP_2
C
Ctnnb1
D
Ctnnb1
Axin2
Expression level
E
Stem cells
Secretory cells
Absorptive cells
Fraction of cells
F
Defensin 5α
Paneth cell numbers per crypt
G
Relative mRNA level
Lyz1
Pla2g2a
Wnt3
Math1
H
G2M cells
I
G2M cells
Proportion of G2M cells
J
Mki67
K
Ki67
Ki67+ cell numbers per crypt
L
EdU/DAPI
EdU+ cell numbers per crypt-villus unit
M
Lyz1
Ang4
Muc2
Mmp7
Fabp6
Apoa1
Fabp2
Reg3b
PC
GC
EEC
N
imEC
mEC

Figure 2

1162 **Figure 2. ieCtnnb1 knockout altered cellular composition and expression**
1163 **profiles of small intestinal crypts.** (A) Schematic illustration of single-cell
1164 sequencing. Crypts were extracted from small intestines followed by
1165 fluorescence activated cell sorting (FACS) to enrich EpCAM+DAPI- epithelial
1166 cells. Cells of two 10-week-old female mice for each genotype were pooled
1167 together to perform single cell transcriptome analyses. (B) UMAP were used to
1168 visualize the clustering of 11,824 single cells from *H11*$^{i.enh}$ mice and 8,094
1169 single cells from *Ctnnb1*$^{\Delta i.enh}$ mice. Cell types were assigned according to
1170 expressions of marker genes. CBC, crypt base columnar cell; TAC, transit
1171 amplifying cell; EEC, enteroendocrine cell; imEC, immature enterocytes; mEC,
1172 mature enterocytes; GC, goblet cell; PC, Paneth cell; TC, tuft cell. (C)
1173 Expression and distribution of *Ctnnb1* in small intestinal crypt cells of *H11*$^{i.enh}$
1174 and *Ctnnb1*$^{\Delta i.enh}$ mice. (D) Violin plots showing the expression of *Ctnnb1* in CBC,
1175 TAC, PC, GC, imEC, mEC; and the expression of *Axin2* in CBC and TAC, of
1176 *H11*$^{i.enh}$ and *Ctnnb1*$^{\Delta i.enh}$ mice. (E) Comparison of the proportion of indicated small
1177 intestinal crypt cell types in *H11*$^{i.enh}$ and *Ctnnb1*$^{\Delta i.enh}$ mice. (F)
1178 Immunohistochemistry (left and middle) and quantification (right) of PCs in
1179 small intestines of *H11*$^{i.enh}$ (n = 6) and *Ctnnb1*$^{\Delta i.enh}$ (n = 6) mice. (G) RT-qPCR
1180 showing relative mRNA levels of PC marker genes (*Lyz1, Pla2g2a, Wnt3,*
1181 *Math1*) in small intestinal crypts of *H11*$^{i.enh}$ (n = 3) and *Ctnnb1*$^{\Delta i.enh}$ (n = 3) mice.
1182 (H) Distribution of G2M cells in *H11*$^{i.enh}$ and *Ctnnb1*$^{\Delta i.enh}$ small intestinal crypts,
1183 based on the expression of cell cycle marker gene *Mki67*. (I) Comparison of the
1184 proportion of G2M cells in CBC and TAC of *H11*$^{i.enh}$ and *Ctnnb1*$^{\Delta i.enh}$ small
1185 intestinal crypts. (J) Violin plots showing the expression of *Mki67* in CBC and
1186 TAC of *H11*$^{i.enh}$ and *Ctnnb1*$^{\Delta i.enh}$ small intestinal crypts. (K)
1187 Immunohistochemistry (left and middle) and quantification (right) of Ki67+ cells
1188 in small intestines of *H11*$^{i.enh}$ (n = 6) and *Ctnnb1*$^{\Delta i.enh}$ (n = 6) mice. (L)
1189 Immunofluorescence (left and middle) and quantification (right) of EdU+ cells
1190 (red) in small intestines of *H11*$^{i.enh}$ (n = 6) and *Ctnnb1*$^{\Delta i.enh}$ (n = 6) mice after 4
1191 hours EdU injection. Nuclei were labeled with DAPI (blue). (M-N) Violin plots
1192 showing expressions of marker genes for secretory cells (*Lyz1, Ang4, Muc2,*
1193 *Mmp7*) and absorptive cells (*Fabp6, Apoa1, Fabp2, Reg3b*) in secretory(M) and

absorptive lineages (N) of *H11*$^{i.enh}$ and *Ctnnb1*$^{\Delta i.enh}$ small intestinal crypts. Scale bars, 50 µm (F, K, and L). Quantification data are shown as means ± SEM, statistical significance was determined using an unpaired two-tailed Student's *t*-test (D, F, J, K, L, M and N). Quantification data are shown means ± SD, statistical significance was determined using Multiple *t*-tests - one per row (G). *$P < 0.05$, **$P < 0.01$, ***$P < 0.001$, and ****$P < 0.0001$. ns, not significant.

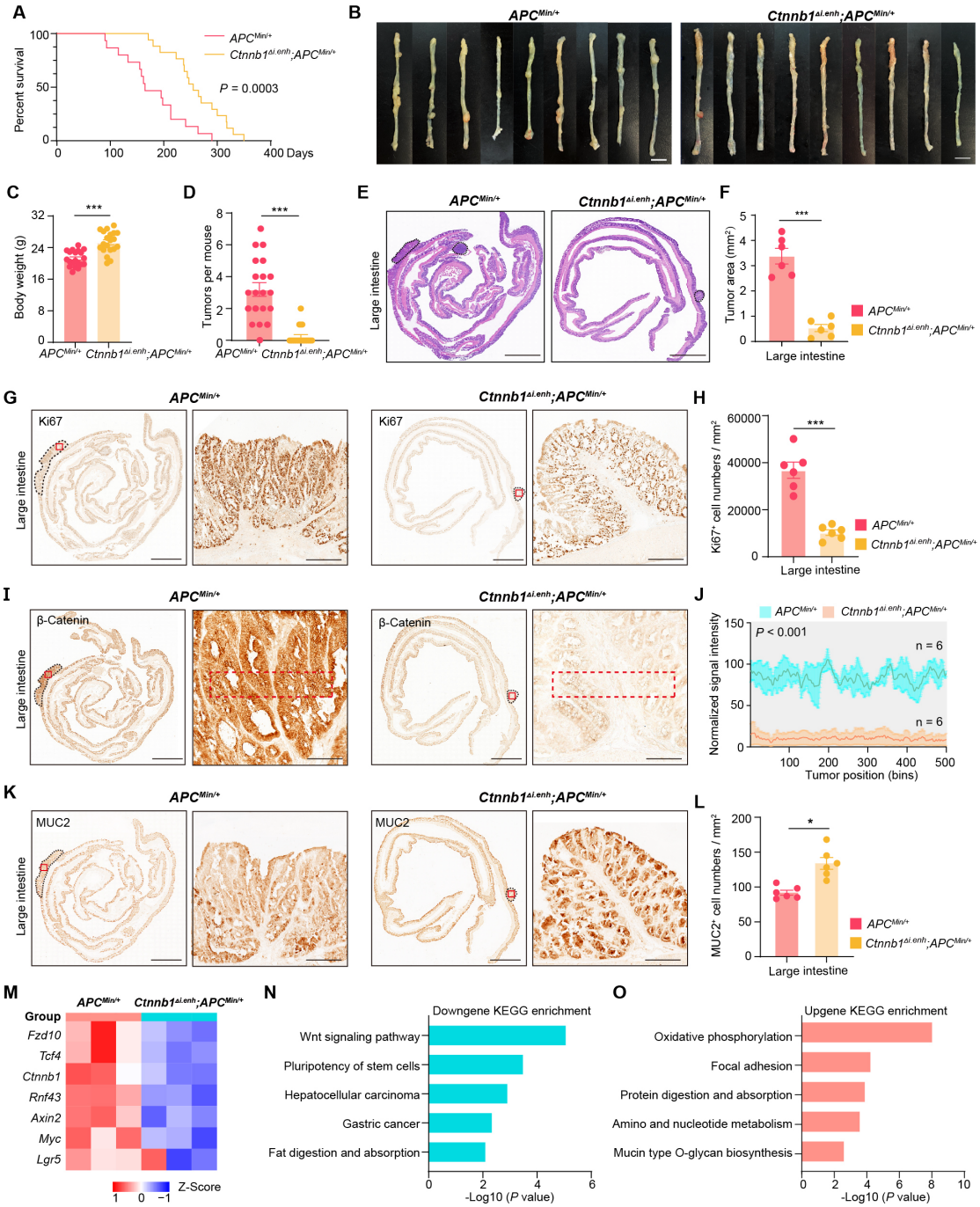

Figure 3

Figure 3. Knocking out ieCtnnb1 inhibits tumorigenesis of colorectal cancer. (A) Survival of *Apc*$^{Min/+}$ (n = 15) and *Ctnnb1*$^{\Delta i.enh}$;*Apc*$^{Min/+}$ (n = 17) mice. (B) Colon images of 5-month-old *Apc*$^{Min/+}$ (n = 9) and *Ctnnb1*$^{\Delta i.enh}$;*Apc*$^{Min/+}$ (n = 9) mice. (C) Weight statistics of 5-month-old *Apc*$^{Min/+}$ (n = 20) and *Ctnnb1*$^{\Delta i.enh}$;*Apc*$^{Min/+}$ (n = 20) mice. (D) The statistical analysis of tumor counts in colons of 5-month-old *Apc*$^{Min/+}$ (n = 9) and *Ctnnb1*$^{\Delta i.enh}$;*Apc*$^{Min/+}$ (n = 9) mice.

(E) Representative H&E staining images of colon sections of 5-month-old *Apc*$^{Min/+}$ and *Ctnnb1*$^{\Delta i.enh}$;*Apc*$^{Min/+}$ mice. (F) The statistical analysis of colon tumor area in 5-month-old *Apc*$^{Min/+}$ (n = 6) and *Ctnnb1*$^{\Delta i.enh}$;*Apc*$^{Min/+}$ (n = 6) mice. (G-H) Immunohistochemistry (G) and quantification (H) of Ki67+ cells in colon tumors of 5-month-old *Apc*$^{Min/+}$ (n = 6) and *Ctnnb1*$^{\Delta i.enh}$;*Apc*$^{Min/+}$ (n = 6) mice. (I-J) Immunohistochemistry (I) and signal intensity statistics (J, red dashed boxes of I) of β-Catenin in colon tumors of 5-month-old *Apc*$^{Min/+}$ (n = 6) and *Ctnnb1*$^{\Delta i.enh}$;*Apc*$^{Min/+}$ (n = 6) mice. (K-L) Immunohistochemistry (K) and quantification (L) of MUC2+ cells in colon tumors of 5-month-old *Apc*$^{Min/+}$ (n = 6) and *Ctnnb1*$^{\Delta i.enh}$;*Apc*$^{Min/+}$ (n = 6) mice. (M) The heat map showing relative expressions of Wnt signaling pathway genes of colon tumors from 5-month-old *Apc*$^{Min/+}$ (n = 3) and *Ctnnb1*$^{\Delta i.enh}$;*Apc*$^{Min/+}$ (n = 3) mice. (N-O) KEGG analyses of downregulated (N) and upregulated (O) genes in colon tumors of 5-month-old *Apc*$^{Min/+}$ (n = 3) and *Ctnnb1*$^{\Delta i.enh}$;*Apc*$^{Min/+}$ (n = 3) mice. Scale bars, 1 cm (B), 4 mm (E, G, I and K), 200 μm (magnified views in G and K), 100 μm (magnified views in I). Quantification data are shown as means ± SEM, statistical significance was determined using an unpaired two-tailed Student's *t*-test (C, D, F, H, J and L) or log-rank analysis (A). *$P < 0.05$, **$P < 0.01$, ***$P < 0.001$, and ****$P < 0.0001$. ns, not significant.

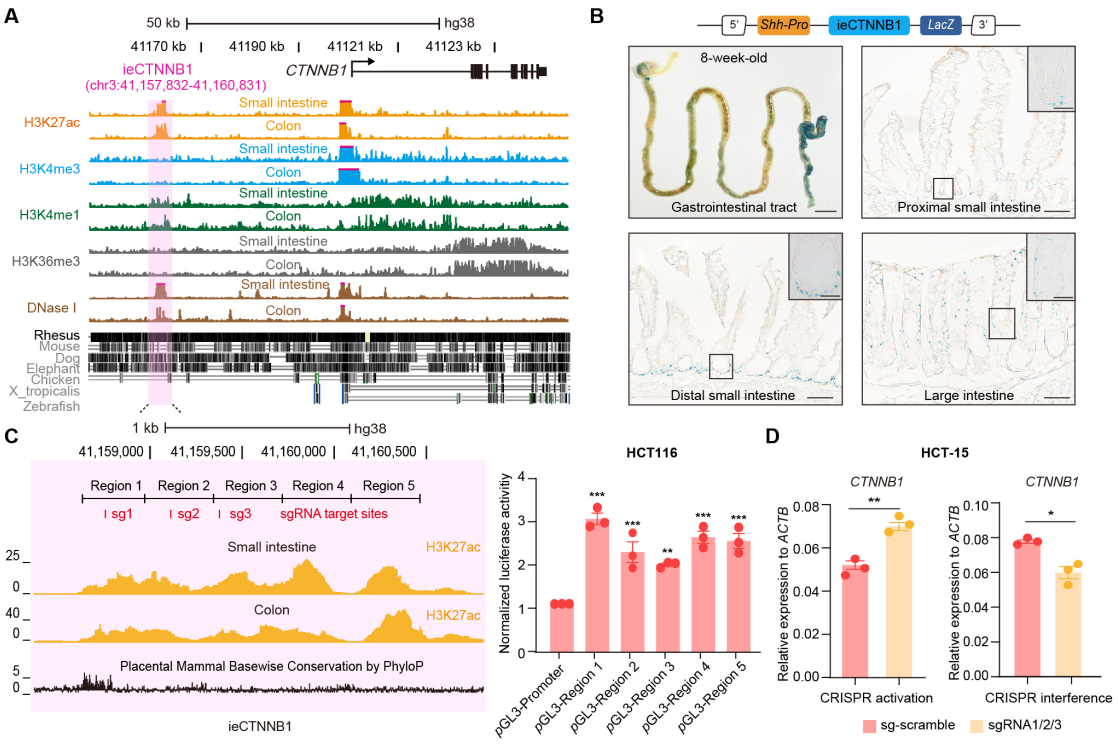

Figure 4

Figure 4. ieCTNNB1 is the intestinal enhancer of human *CTNNB1*. (A) Schematic representation of human *CTNNB1* gene and the location of ieCTNNB1 (3,000 bp, pink shading), which is marked by H3K27ac and H3K4me1 peaks, and DNase Ⅰ hypersensitivity in human small intestine (30-year-old female) and colon (34-year-old male). Data were obtained from ENCODE. (B) Top: a schematic illustration showing that the knock-in construct containing the *Shh* promoter, ieCTNNB1 sequences (3,000 bp), and the LacZ reporter gene. Bottom: X-Gal staining (blue) of the gastrointestinal tract, and sections of the proximal small intestine, distal small intestine, and large intestine in 8-week-old *H11*$^{hi.enh}$ mice. (C) Left: ieCTNNB1 is marked by enrichment of H3K27ac in human small intestine (30-year-old female) and colon (34-year-old male). Data were obtained from ENCODE. Locations of sgRNA target sites were indicated. Five subregions of ieCTNNB1 were shown. Right: luciferase reporter assay in HCT116 cells transfected with indicated plasmids for 48 hours. (D) RT-qPCR showing relative mRNA levels of *CTNNB1* in HCT-15 cells transfected with indicated CRISPR activation or CRISPR interference vectors

1245 for 48 hours. Scale bars, 1 cm (whole mount in B), 100 µm (sections in B), 10
1246 µm (magnified views in B). Quantification data are shown as means ± SEM,
1247 statistical significance was determined using one-way ANOVA analysis (C) and
1248 an unpaired two-tailed Student's *t*-test (D). *$P < 0.05$, **$P < 0.01$, ***$P < 0.001$,
1249 and ****$P < 0.0001$. ns, not significant.
1250

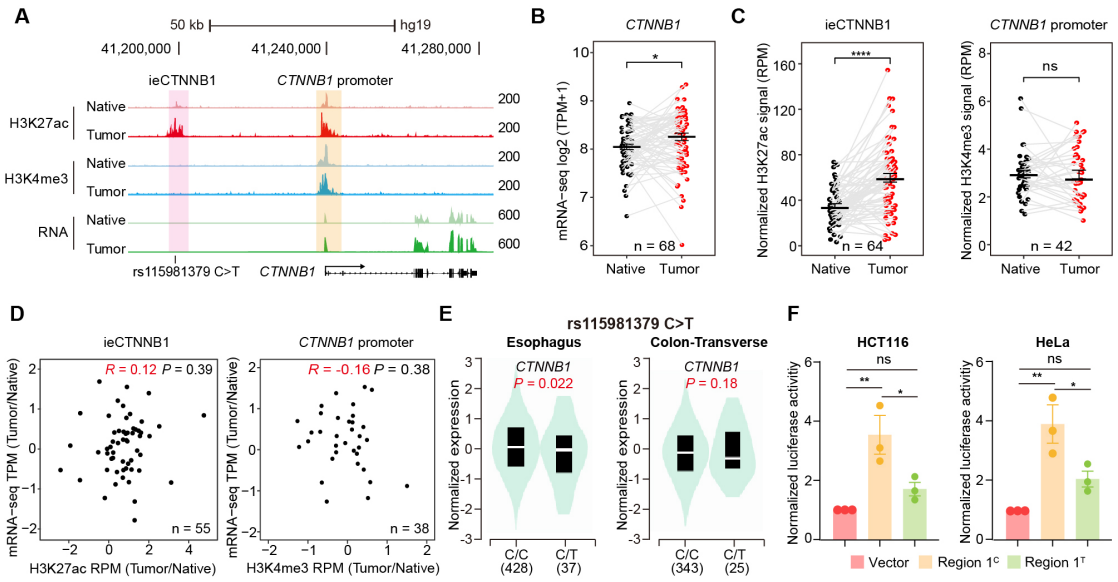

Figure 5

Figure 5. ieCTNNB1 is activated in colorectal cancer and its activity positively correlates with the expression of *CTNNB1*. (A) Schematic representation of ieCTNNB1 (pink shading) and *CTNNB1* promoter (yellow shading), which is respectively marked by H3K27ac and H3K4me3 peaks, and mRNA signals in native and tumor tissues of a patient with colorectal cancer. The location of risk mutation site was indicated. (B) Comparison of *CTNNB1* expression levels in native and tumor tissues of colorectal cancer patients (n = 68). (C) Left: comparison of H3K27ac signals at ieCTNNB1 in native and tumor tissues of colorectal cancer patients (n = 64). Right: comparison of H3K4me3 signals at *CTNNB1* promoter in native and tumor tissues of colorectal cancer patients (n = 42). (D) Left: correlation between H3K27ac signals at ieCTNNB1 and *CTNNB1* expression in native and tumor tissues of colorectal cancer patients (n = 55). Right: correlation between H3K4me3 signals at *CTNNB1* promoter and *CTNNB1* expression in native and tumor tissues of colorectal cancer patients (n = 38). (E) Left: comparison of *CTNNB1* expression in esophagus between subjects with common sequence (C/C, n = 428) and variant sequence (C/T, n = 37). Right: comparison of *CTNNB1* expression in transverse colon between subjects with common sequence (C/C, n = 343) and

variant sequence (C/T, n = 25). (F) Luciferase reporter assay in HCT116 and HeLa cells transfected with indicated plasmids for 48 hours. Quantification data are shown as means ± SEM, statistical significance was determined using a paired (B, C and D) or unpaired (E) two-tailed Student's *t*-test and Two-way ANOVA analysis (F). *$P < 0.05$, **$P < 0.01$, ***$P < 0.001$, and ****$P < 0.0001$. ns, not significant. R: Pearson correlation.

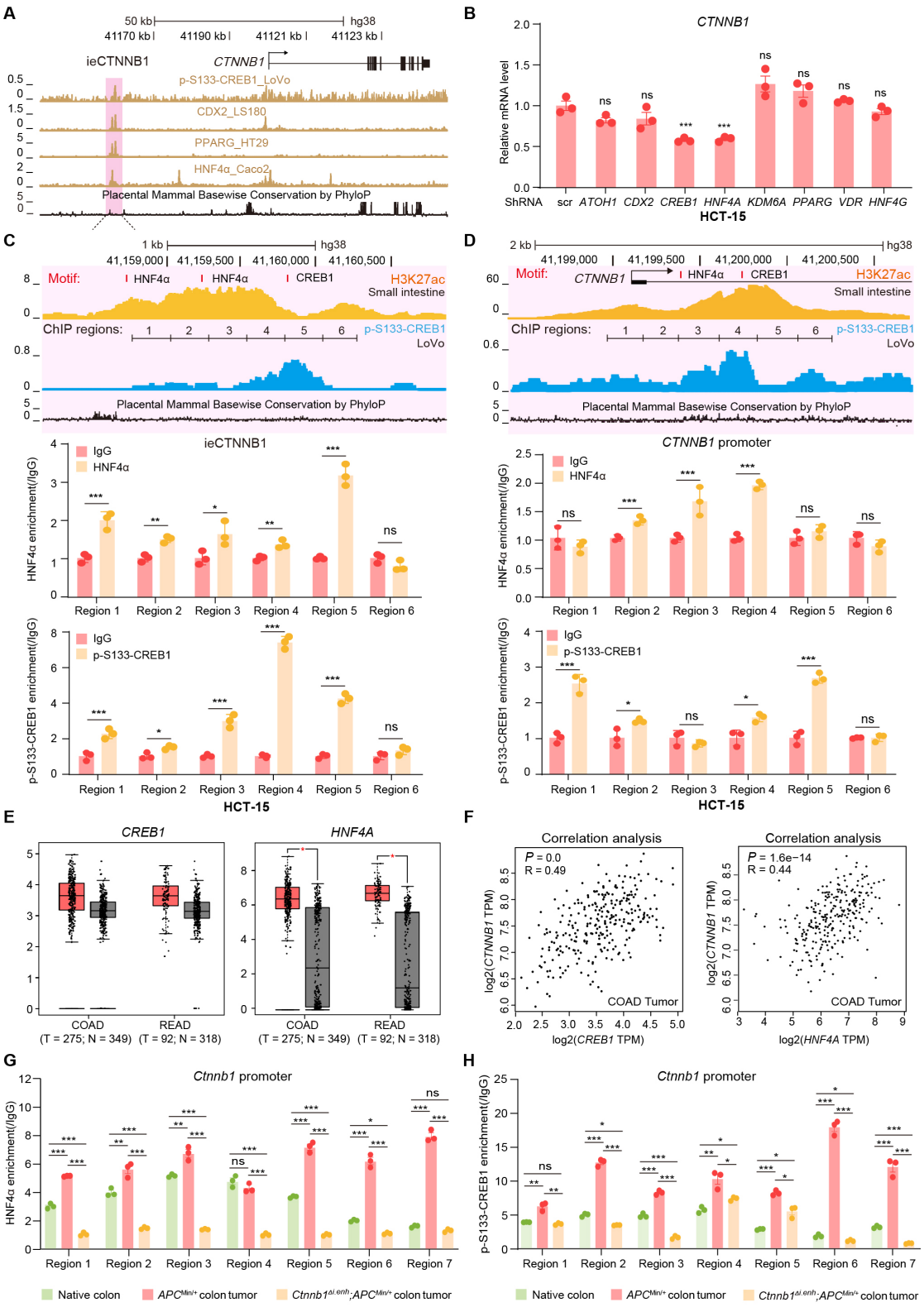

Figure 6

Figure 6. HNF4*α* and p-S133-CREB1 associate with ieCTNNB1 to regulate *CTNNB1*'s transcription. (A) ChIP-seq tracks of indicated trans-acting factors enriched at ieCTNNB1 (pink shading) in indicated colorectal cancer cell lines.

(B) RT-qPCR showing relative mRNA levels of *CTNNB1* in HCT-15 cells transfected with indicated shRNA-expressing plasmids for 48 hours. The expression level of *CTNNB1* in cells transfected with scramble (scr) shRNA was set to '1'. (C-D) Top: schematic diagram showing the enrichment of H3K27ac and p-S133-CREB1 at ieCTNNB1 (C) and *CTNNB1*'s promoter (D). Locations of HNF4α and CREB1 binding motif sites were indicated. Middle and bottom: ChIP-qPCR showing enrichment of HNF4α (middle) and p-S133-CREB1 (bottom) at ieCTNNB1 (C) and *CTNNB1*'s promoter (D) in HCT-15 cells. Locations of ChIP regions were indicated. (E) Comparison of expression levels of *CREB1* and *HNF4A* between native and tumor tissues in colon adenocarcinoma (COAD) and rectum adenocarcinoma (READ) tumors. (F) Correlations between the expression level of *CTNNB1* and those of *CREB1* or *HNF4A* in COAD tumors. (G-H) ChIP-qPCR showing enrichment of HNF4α (G) and p-S133-CREB1 (H) at *Ctnnb1* promoter in native colon tissues of WT (n=3) mice, tumor tissues of $Apc^{Min/+}$ (n=3) mice and $Ctnnb1^{\Delta i.enh}$;$Apc^{Min/+}$ (n=3) mice. Quantification data are shown as means ± SEM, statistical significance was determined using one-way ANOVA analysis (B), unpaired two-tailed Student's *t*-test (E and F) and Multiple *t*-tests - one per row (C, D, G and H). *$P < 0.05$, **$P < 0.01$, ***$P < 0.001$, and ****$P < 0.0001$. ns, not significant. R: Pearson correlation.